# THE INTERFACE RESPONSE FUNCTION AND MELTING POINT OF THE PRISM INTERFACE OF HEXAGONAL ICE USING A FLUCTUATING CHARGE MODEL (TIP4P-FQ)

A Thesis

Presented to the Faculty of the Graduate School

of Cornell University

In Partial Fulfillment of the Requirements for the Degree of

Master of Science

by

Benjamin Ferrers Nicholson

May 2006

# ABSTRACT

Molecular Dynamics simulations have been used to follow the rate of growth and recession of the prismatic surface of a hexagonal ice-water interface. The fluctuating charge, four-site transferable intermolecular potential model, TIP4P-FQ, was used at temperatures between 265 K and 310 K in a series of isobaric isothermal (NPT) Molecular Dynamics simulations. Using appropriate order parameters, an interface response function that captures the speed of the moving interface as a function of temperature was constructed that covers the melting and growth of hexagonal ice. From the interface response function ($T_v$=0), the melting temperature was found to be 303 ± 8 K and the maximum crystallization velocity was estimated to be ~1 m/s at 260 K (14% undercooling; in line with the kinetics of other systems such as Si). Changing the Lennard-Jones σ parameter from 3.159Å to 3.173 Å, in line with a previous parameterization by Rick, confirms results from Gibbs-Duhem integration that predicted a reduction in the melting temperature to 276 K. While this value corresponds well with experiments, given the relative simplicity of the model, it comes at the expense of accurately predicting the properties of liquid water. Crystallization from the prism interface involves at least two layers, as determined by density and dipole analysis and is in line with results found from previous TIP6P results.

# BIOGRAPHICAL SKETCH

Benjamin Ferrers Nicholson was born in Marin County, California on December 27, 1980. He was the valedictorian and homecoming king of the Redwood High School Class of 1999, and became a student at the Massachusetts Institute of Technology that same year. He joined the Phi Kappa Sigma Fraternity in 2000. He graduated in 2003 with a bachelor's degree in Chemical Engineering with a minor in Economics. He entered the graduate program at the School of Chemical and Biomolecular Engineering at Cornell Engineering in August 2003. He worked in Professor Paulette Clancy's research group, which concentrates in advanced material computer simulation.

This thesis is dedicated to my parents, William and Carland, who recognized that I was becoming a chemical engineer long before I did.

# ACKNOWLEDGEMENTS

I am thankful for all the people who supported me through my three years here. Their participation has made my experience here not only possible, but also memorable.

I am extremely grateful to Professor Paulette Clancy. She introduced Molecular Dynamics to me in the Advanced Chemical Engineering Thermodynamics class, encouraging in me an enthusiasm for the concept. As my advisor, she demonstrated great patience and provided excellent guidance as I developed a proficiency in computer simulations. Her counsel in preparing papers and presentations has proved invaluable. My experience at Cornell would have been neither as rewarding nor as enjoyable without her.

Professor Steven Rick of the University of New Orleans jump-started my research. In the summer of 2004, he demonstrated and gave to me the molecular dynamics code of the water model I used for my project. He continued to support my work from a distance, explaining unique features of his code and complementing my findings with those from a modified water model. Professor Lawrence Cathles provided the opportunity for me to explore gas hydrates from a geologic perspective. Continued involvement with him in the Department of Earth and Atmospheric Sciences has quite literally changed the way I look at the world. Professor A. Brad Anton kept me on my toes. His advice on theoretical models reminded me that molecular simulation is not the last word in science.

Devashish Choudhary, Chin-Lung Kuo, Erik Albenze, Leonard Harris, Mohit Haran, Jay Catherwood, Joesph Goose and Michelle Giron all clocked hours with me

in Olin 365. Their welcome company made the hours fly in discussions that ranged from coding techniques and approaches to baseball, football, and cricket chatter.

Finally, I am thankful for everyone who made Ithaca such a wonderful place to live. Carol Scheele kept a careful a watch over my well-being, as she did for my sister before me. My roommates Robert Kuczenski, Conor Foley and Michael Durst endured my numerous idiosyncrasies, and helped make Ithaca home. The camaraderie within the School of Chemical Engineering has made my experience here a special one, from the confines of Olin Hall, to the picnic table at Willard Way, to the poker tables down the hill, to the frozen seats at Ralph Wilson Stadium. I thank you all.

TABLE OF CONTENTS

LIST OF FIGURES

LIST OF TABLES

# Chapter 1

# Introduction

The kinetics of crystallization at an interface is difficult to investigate experimentally. The interface between solid and liquid is very thin, less than 10 Å wide, and maintains a steady balance of adsorbing and desorbing molecules even at equilibrium conditions; outside of those conditions it is either growing or melting. One of the best known examples of crystallization is the transition of liquid water to solid ice.

Preventing or encouraging the crystallization of water has many applications. It is crucial to prevent ice growth on airplane wings during flight [1]. Quick freezing of foods prevents formation of ice crystals and maintains food quality and flavor [2]. Some insects and fish have anti-freeze proteins that inhibit ice growth, preventing cell membrane rupture during cold seasons [3]. Gas hydrates, in which small molecules such as methane or carbon dioxide are trapped in a crystalline clathrate cage of water molecules, can be viewed as a hazard through unwanted crystallization in gas transmission lines and an environmental threat through sudden melting with the subsequent release of greenhouse gases [4]. Hydrates can also provide a potential source of energy by the release of the entrapped natural gas or as a route to sequestering carbon dioxide as a potential carbon sink. While water is one of the best studied chemicals on the planet, basic characteristics of water, such as the hydrogen bonding structure of its first coordination shell, are still uncertain [5–8]. More needs to be known about the crystallization and interface characteristics of water to better understand freezing processes.

The existence of anisotropy in the crystal growth of ice at different interfaces has only recently begun to be explored [9]. While the melting temperature of the different faces of ice is the same, the rate at which crystallization happens is dissimilar, as are the mechanisms of melting. These differences have not been fully characterized.

Computer simulation techniques provide a better understanding of the solid-liquid interface of water. Using Molecular Dynamics simulations to study the movement of water molecules, time can be modeled on a femtosecond timescale, allowing detailed information on structure and properties to be analyzed at the atomic level. Simulations of significantly sub-cooled liquids or very fast reactions pose no significant challenge. However, Molecular Dynamics simulations also have several drawbacks. Computing power limits simulations to several thousand molecules for times no longer than a few nanoseconds. Nevertheless, these simulations can yield valuable information that experiments lack the delicacy to divulge.

## 1.1 Motivation

As one of the most ubiquitous chemicals on the planet, water has been simulated using dozens of computer models [10] for hundreds of purposes in a variety of conditions, from carbon nanotube interaction [11] to involvement in protein structure [12] to supercritical hydrolysis of cellulose [13]. A model's ability to calculate known properties at different conditions for which it was not initially parameterized to predict is a common measure of the effectiveness and robustness of a model. Despite the plethora of models, none is clearly superior, leading to continued efforts to find better models.

The TIP4P-FQ model for water-water interaction [14] is relatively new. The dipole moment of water is different in different phases [15–17], and the fluctuating charge can effectively model this characteristic, making it a potential improvement over other models for use in situations involving phase changes [14]. While several properties of TIP4P-FQ water have been established [18], the melting temperature of the common hexagonal ice polymorph has not yet been established. This thesis will determine the melting temperature of this model to assist in the determination of the usefulness of this model for low-temperature situations.

The kinetics of water crystallization are largely unknown. The difficulties of maintaining a sub-cooled liquid make development of empirical results an ordeal. The velocities of a solid-liquid interface for a range of temperatures, known as the interface response function, can be determined using Molecular Dynamics [19]. The first interface response function of water using Molecular Dynamics was completed recently [9], and only for a small interval of temperatures. While the stable solid-liquid interface has been well characterized using a variety of models [20–22], the characteristics of a growing ice interface have received far less attention. Our portrayal here of the interface response function and examination of the changes in density and dipole moment in the interface will lead to a better understanding of the freezing process of water.

## 1.2 Thesis Organization

This work determines the melting temperature and the kinetics of interface crystallization for the prismatic interface of hexagonal ice and liquid for the TIP4P-FQ model of water. Molecular Dynamics simulations are applied to solid-liquid-solid

water system at different temperatures, and the interface response is measured and characterized. Prior to this work, information relevant to the interface response function of water has been only investigated in rudimentary fashion [9,23]. This provided the motivation for a detailed study of the motion of a solid-liquid water interface over a wide range of temperatures.

The next chapter presents the techniques used for the execution and analysis of the computer simulations performed for this thesis. We provide a discussion of the Molecular Dynamics method and include a brief history of water models. We describe the geometric structure and the Lennard-Jones and Columbic interaction potentials of the TIP4P-FQ model, including an explanation of Ewald sums and fluctuating charges. The initial set-up of the simulation is constructed to restrict the effects of the limitation to consider a physically small system in determining bulk properties. We explain how to discern a liquid molecule from a solid molecule, which is crucial to the derivations of the conclusions of this thesis, and provide the classification procedure used in this thesis. Advances in our understanding of interface growth in ice-water systems obtained from previous simulations and experiments not only provide a foundation for this work, but also show the vast uncharted area in understanding ice-water interfaces. We describe methods used to determine the melting point of water and confirm the consistency of the methods. The concept of an interface response function and the application of the Wilson-Frenkel equation to establish the melting point and the maximum freezing velocity are reviewed here.

The results of the interface response function for ice are presented in Chapter 3. The suitability of the set-up is confirmed by comparison of self-diffusivities to previous results. We use the movement of the ice-water interface to

predict the melting point and the freezing kinetics of TIP4P-FQ water. The nature of the solid-liquid interface is characterized together with a study of the solid and liquid phases and the moving interface, which are illustrated in terms of density and dipole profiles. The mechanism of prismatic growth is determined by the width of the interface and changes in density and dipole profiles with a moving interface. The melting temperature of a modified TIP4P-FQ model, as previously determined by Gibbs-Duhem integration, is confirmed by results using the interface response function.

The conclusions of this work are given in chapter 4. The melting temperatures of various water models are compared to their temperatures of maximum densities, and comparisons are made to silicon and germanium, whose crystal structures are also tetrahedral in nature. Further recommendations for future work are given, particularly in the field of natural gas hydrates.

# Chapter 2

# Simulation Details

This chapter describes the Molecular Dynamics method of computer simulation. Basic principles are introduced and the evaluations of some thermodynamic properties relevant to a study of the solid-liquid interface are described. The TIP4P-FQ model, a 4-site interaction water model with a fluctuating columbic charge, is selected from a variety of popular water models because of its variable dipole moment. The initial setup of water molecules is based on a Hayward and Reimers unit cell that results in an ice-water-ice configuration with prismatic interfaces. The diffusivity constant of the liquid phase is used to confirm the validity of this simulation in comparison to previous studies. Determination of whether an individual water molecule is in a solid-like or liquid-like environment is used to locate and characterize the ice-water interface. The movement of the two interfaces as a function of time reveals the interface velocity function, which can be used to determine the melting point of the TIP4P-FQ model of water (the point at which the velocity of the growth front is zero), and the temperature and speed of the maximum crystallization velocity.

## 2.1 Molecular Dynamics

Molecular Dynamics is a numerical simulation technique used to solve the equations of motion for atoms by finite difference methods [24]. For a system of atoms with Cartesian coordinates, $\vec{r}_i$, and masses, $m_i$, their movements can be determined by the forces, $\vec{F}_i$, in Newton's second law:

$$\vec{F}_i = m_i \ddot{\vec{r}}_i \tag{2.1}$$

The forces that act on the particles originate from the interaction potential, $\phi$, that exists between the particles:

$$\vec{F}_{ij} = \nabla \phi_{ij} \tag{2.2}$$

The configuration energy of the system, U, is the sum of all pairwise interaction energies:

$$U = \sum_{i}^{N-1} \sum_{j>i}^{N} \phi_{ij} \tag{2.3}$$

Potential energy is assumed to be based on two-body interactions.

The most common method of solving the equations of motion is to use the Verlet algorithm [25]. Employing Taylor expansions of equation 2.1, this algorithm predicts in the next time step, $\delta t$, a particle's position in space, $\vec{r}_i(t+\delta t)$, based on its current and previous time step, $\vec{r}_i(t)$ and $\vec{r}_i(t-\delta t)$, and its acceleration, $\ddot{\vec{r}}_i(t)$:

$$\vec{r}_i(t+\delta t) = 2\vec{r}_i(t) - \vec{r}_i(t-\delta t) + \delta t^2 \ddot{\vec{r}}_i(t) \tag{2.4}$$

The velocity of the particle, and consequently its kinetic energy, can then be calculated:

$$\dot{\vec{r}}_i = \frac{r(t+\delta t) - r(t-\delta t)}{2\delta t} \tag{2.5}$$

The Verlet algorithm is time–reversible, and has errors on the order of $\delta t^4$; the velocity equation has errors on the order of $\delta t^2$.

Different macroscopic constraints result in different ensembles of the system. The constant pressure, constant temperature ensemble (NPT) is of particular interest here, as it best represents common experimental settings.

The energy of the system can exchange energy with a large heat reservoir, fixing the temperature of the system. The Nosé-Hoover algorithm [26] rescales the velocities of the system particles with a heat reservoir parameter, $s$, and a thermal inertia parameter, $Q_{NH}$:

$$\ddot{\vec{r}}_i = \vec{F}_i / m \cdot s^2 - 2\dot{s}\dot{\vec{r}} / s \tag{2.6}$$

$$Q_{NH}\ddot{s} = \sum_i m\dot{\vec{r}}_i^{\,2} s - (f+1)k_B T / s \tag{2.7}$$

where $f$ is the number of degrees of freedom, $k_B$ is Boltzmann's constant and $T$ is the fixed temperature. System temperature is calculated from the kinetic energy of the particles, $K$:

$$\mathrm{T} = 2K / Nk_B \tag{2.8}$$

where N is number of particles in the system.

The pressure can be held constant by coupling the system to the volume of the box, V. The Andersen algorithm [27] imitates the presence of a piston with mass, $Q_A$, acting on the box. The positions and velocities of the particles are rescaled by a pressure parameter, $\vec{s}_A$:

$$\vec{r}_i = V^{1/3}\vec{s}_{Ai} \tag{2.9}$$

$$\dot{\vec{r}}_i = V^{1/3}\dot{\vec{s}}_{Ai} \tag{2.10}$$

where the equations of motion for s and V are:

$$\ddot{\vec{s}}_{Ai} = \vec{F}_i \Big/ mV^{1/3} - \tfrac{2}{3}\dot{\vec{s}}\dot{V}\Big/ V \tag{2.11}$$

$$\ddot{V} = (\mathrm{P} - P)/Q_A \tag{2.12}$$

The force, $\vec{F}_i$, and the instantaneous pressure, P, are calculated from unscaled coordinates and momenta. Pressure is the sum of kinetic and force contributions:

$$\mathrm{P} = \rho k_B \mathrm{T} + \frac{1}{3V}\sum_{i}^{N-1}\sum_{j>i}^{N}\vec{F}_{ij}\cdot\vec{r}_{ij}\ , \tag{2.12}$$

where $\rho$ is the number density.

Periodic boundaries of the simulation cell are applied to prevent the presence of walls or vacuums [24]. For those dimensions where a periodic boundary is simulated, particles near a dimension's boundary interact with images of the particles situated at the opposite side of the dimension. Simulation box dimensions are allowed to fluctuate independently [28].

## 2.2 Water Models and the TIP4P-FQ Model

At least different 48 interaction potentials have been developed to simulate the water molecule [10,29,30]. A model's ability to determine known physical properties lends

merit to its talent to predict unknown phenomena. For water, density and distribution functions derived from x-ray scattering and neutron diffraction are typically used for this sort of comparison. This large number of existing models suggests that no single model is superior. Indeed, increases in accuracy typically require a larger computational cost, more parameters, or a smaller applicable range of temperature and pressure [29]. A model may be tailored for specific applications, but is likely to be inaccurate in situations well outside the properties of environments in which its parameters were fitted.

Water models of the SPC and TIPS families are among the most popular for water simulation among researchers. The addition of elements such as Ewald sums and fluctuating charges allows for a better definition of the interaction potential between molecules. The TIP4P-FQ model replaces the static point charge of the TIP4P model with a fluctuating charge that responds to the local electrostatic field. This modification makes it more suited for heterogeneous environments, such as the phase change from solid to liquid of interest here.

### 2.2.1 The Development of Water Models

Water has been investigated by numerical techniques more than any other liquid [10]. The first interaction potential model by Bernal and Fowler [31] actually predates the Metropolis Monte Carlo technique [32] by twenty years. Water's ubiquitous nature has made an understanding of water crucial in research ranging from gas hydrates to biological processes to industrial applications to meteorological processes. The extreme range of environments in which water is present has led to the development of

dozens of water models, each with their own unique traits. Most models, however, fall within a few easily definable categories.

Basic semi-empirical water models consist of columbic and Lennard-Jones interactions. The columbic potential is an electrostatic force proportional to the magnitude of the charges involved and inversely proportional to the distance between them:

$$\phi_{Cij} = \frac{1}{4\pi\varepsilon_0}\frac{q_i q_j}{|\vec{r}|^2}\hat{r}, \tag{2.13}$$

where $\varepsilon_0$ is the permittivity of free space. The Lennard-Jones potential is a mathematical model which describes an attractive van der Waals force at long distances and a Pauli repulsion force at short distances that results from overlapping orbitals:

$$\phi_{LJij} = 4\varepsilon\left[\left(\frac{\sigma}{\vec{r}_{ij}}\right)^{12} - \left(\frac{\sigma}{\vec{r}_{ij}}\right)^{6}\right] \tag{2.14}$$

The well depth, $\varepsilon$, and the hard sphere radius, $\sigma$, can be parameterized either empirically or analytically. While the Lennard-Jones potential is an approximate model, its general ability to predict correct trends and its simplicity make it an attractive choice.

Typically, the Lennard-Jones potential is centered on the oxygen atom. The charge distribution on the water molecule varies depending on the geometry of the model (Figure 2.1). For a three-site model (SPC, TIP3P) a negative charge is placed on the oxygen site and equal positive charges are placed on the hydrogen sites. For a four-site model (BF, TIP4P), the negative charge is placed on a fictitious M-site found

along the bisector of the HOH angle. The five-site model (ST2, TIP5P) moves the negative charge to a pair of L-sites; the LOL and HOH angles share the same bisector, but the plane of the LOL angle is perpendicular to the HOH angle. Six-site models (TIP6P) contain both L-sites and the M-site.

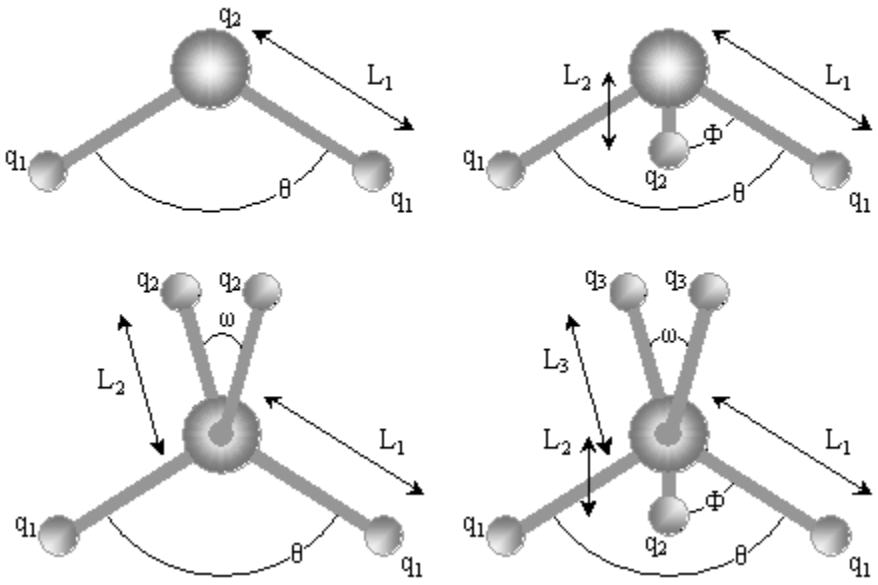


Figure 2.1. Three-, four-, five- and six- site model representations of a water molecule.

Most potentials are semi-empirical. Charges are often chosen to reproduce the dipole moment, and bond angles and lengths are modified to represent averages of the water structure in different phases (TIP4P) or to encourage the stability of certain crystal lattices (ST2).

Additional complexities can be added to the design of water models to better capture the interaction in a system. These include Ewald sums, flexibility, and polarizability. Ewald sums reduce the columbic interaction between an ion and all its

periodic images to two gaussian charge distributions of equal magnitude and opposite sign. This can have a dramatic effect on model properties. The application of Ewald sums to the SPC/E potential raised the prediction of the melting point of hexagonal ice from 190 K [33] to 279 K [34]. Reparameterization of the SPC model to include Ewald sums results in a melting temperature of about 220 K [23,33,35]. Flexibility and polarizability allow for a change in the water dipole by changing the geometry or the magnitude of the charges, respectively. As phase changes include marked changes in the dipole moment of water, models that include one of these characteristics are favored in principle.

### 2.2.2 The TIP4P-FQ Model

The fluctuating charge reflects the movement of charge on the water atoms, which changes significantly during thermodynamic state transitions. This makes the TIP4P-FQ model particularly desirable for dynamic heterogeneous environments, where mean field charge values cannot be applied with accuracy [14]. Charge is distributed throughout the water molecule such that the electronegative values are equal. When outside electrostatic potentials perturb the molecule, the charge is redistributed. This is achieved by assigning the charges fictitious masses, velocities and energies, then subjecting them to Newtonian mechanics. The model accurately produces the temperature of the maximum density of real water, but gives high values for solid densities and the heat of sublimation. It predicts the correct dipole moment in a variety of phases, without the computational cost of polarizable models (the re-evaluation of charge increases computation by only 10%).

The TIP4P-FQ model has the same physical dimensions as the TIP4P model (Figure 2.2, Table 2.1). Only the variable charge on the hydrogen sites and the M site are different. The charges fluctuate in response to a change in the surrounding electrostatic potential, whether due to its movement or the movement of other molecules. Each molecule is constrained to be neutral, such that charge cannot be transferred between molecules, but only from atom to atom within a molecule:

$$\sum_{\alpha=1}^{N_{atoms}} Q_\alpha = 0 \tag{2.15}$$

The difference between electronegativities of atoms within the molecule causes change in charge fluctuation, $\ddot{Q}_\alpha$:

$$M_Q \ddot{Q}_\alpha = -\frac{1}{N_{atom}} \sum_{\beta=1}^{N_{atom}} (\tilde{\chi}_\alpha - \tilde{\chi}_\beta) \tag{2.16}$$

where $\tilde{\chi}$ is the Mulliken electronegativity and $M_Q$ is a conjured charge mass, with units of (energy time$^2$)/charge$^2$. A charge mass of $6.0\times10^{-5}$ is sufficiently small to allow for rapid adjustments in charge, yet large enough that a femtosecond timestep adequately captures the solution of the equations of motion.

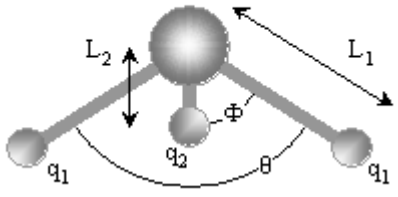


Figure 2.2. Structure of the TIP4P-FQ water model.

Table 2.1. Parameters of the TIP4P-FQ water model.

| Parameter | $\sigma$ | $\varepsilon$ | $L_1$ | $L_2$ | $\theta$ | $\Phi$ |
|---|---|---|---|---|---|---|
| Value | 3.15365 Å | 0.6480 kJ/mol | 0.9572 Å | 0.15 Å | 104.52° | 52.26° |

The energy of a TIP4P-FQ molecule is the sum of the Lennard-Jones energy, the intermolecular Coulomb energy, and an intramolecular self-energy. The Lennard-Jones interaction is measured only between oxygen sites. Electrostatic interactions are measured between the hydrogen sites and the M-sites, bisecting the H-O-H bond angle 0.15 Å from the oxygen sites. Ewald sums are applied to the columbic interaction. The Lennard-Jones and electrostatic parameters have been adjusted to obtain the correct gas-phase dipole moments, as well as to optimize the liquid phase energy, pressure and pair correlation functions.

The TIP4P-FQ accurately models the temperature of maximum density, and the dipole moments in the gas, liquid, and hexagonal ice phases. For these reasons, the TIP4P-FQ model was chosen for use in this interfacial crystallization study.

## 2.3 Initial Simulation Setup

Hexagonal ice, also known as ice $I_h$, is a crystalline structure of the space group $P6_3/mmc$, with four water molecules per unit cell. Oxygen atoms lie on two intersecting hexagonal lattices, with a hydrogen atom between each pair of oxygen atoms. Like nearly all other phases of ice, hexagonal ice obeys the ice rules: each water molecule has four hydrogen-bonded nearest neighbors, with each two hydrogen atoms near each oxygen atom, one on each oxygen-oxygen bond. The combination of

two hydrogen atoms along four oxygen-oxygen bonds allows for 6 possible orientations for a water molecule, and 24 unique orientations in the unit cell. In a disordered lattice, the orientations of the hydrogen atoms are random, such that the net electric multipole moments of the charge distribution are zero. In the simulation, the number of molecules in the lattice is small enough that a simple random distribution cannot ensure a null charge. Electric multipole moments in a unit cell must be kept to a minimum to reduce long–range interactions [36].

The Hayward and Reimer method [37] for the representation of ice $I_h$ periodic lattices has zero net dipole moment and selects for a minimal quadrupole moment. Each of the 24 possible unit cells orientations occur an equal number of times to ensure zero dipole moment; these lattices are then screened for zero quadrupole moment and relatively low octupole moment. Lattices of varying size can be created using this method.

The initial configuration of the periodic simulation box was created with the 5 x 3 x 3 orthorhombic unit cell of ice from Hayward and Reimers, containing 360 molecules in a proton-disordered structure, with a zero net dipole and a zero net quadrupole moment. This structure was equilibrated at 280 K and a pressure of 1 atm. Three additional copies of this cell were then placed end-to-end against the prismatic $\{10\bar{1}0\}$ face, creating an ice box consisting of 1440 water molecules and approximately 80Å by 20Å by 20Å, its longest dimension perpendicular to the c axis. The prismatic face was chosen for study because ice crystallization from this face (known as S2 ice) is faster than that from the basal {0001} face (known as S1 ice) [38]. Growth from the secondary prismatic $\{11\bar{2}0\}$ face is at least as fast as the prismatic face, but previous simulation work with the TIP6P model of water suggests that the secondary prismatic face grows into the primary prismatic face [9].

The desired ice-liquid-ice system was created by fixing the positions of the water molecules in the terminal 5 x 3 x 3 boxes, while the inner two were melted by simulating a temperature of 400 K for 20 ps, followed by cooling for 40 ps to 298 K by adjusting the temperature in intervals. Finally, the atoms in the ice portions of the system were allowed to move and the whole system was simulated for 300 ps to 280 K, creating an ice-water-ice system shown in Figure 2.3. The reduction in the water section from one-half the size of the simulation to about one-third in Figure 2.3 already suggests ice growth at 280 K.

Figure 2.3. Initial configuration of ice-water-ice system, basal view. Oxygen atoms are black, hydrogen atoms are white. The c-axis (basal face) comes out of the page.

## 2.4 Self-Diffusivity in Molecular Dynamics

The self-diffusivity of TIP4P-FQ water over a range of temperatures has already been established by Rick [18] using a periodic box with 256 water molecules. However, calculation of the diffusion constant can be used as a confirmation that the model remains valid in the larger simulation.

Self-diffusivity is the spontaneous movement of particles in an environment where only those particles exist. The self-diffusivity of liquid water over a range of

temperatures has been fitted empirically to the form $D = D_o T^{1/2}\left(T/T_S - 1\right)^{\gamma}$, where $D$ is the diffusion coefficient. For a three-dimensional system, the diffusion constant is defined as

$$D = \tfrac{1}{3}\int_0^{\infty} dt \left\langle \vec{v}_i(t) \cdot \vec{v}_i(0) \right\rangle, \tag{2.17}$$

where $\vec{v}_i(t)$ is the velocity of a molecule's center of mass at time *t.* The corresponding Einstein relation, which holds true for long *t*, is

$$2tD = \tfrac{1}{3}\left\langle \left|\vec{r}_i(t) - \vec{r}_i(0)\right|^2 \right\rangle, \tag{2.18}$$

where $\vec{r}_i(t)$ is the position of a molecule's center of mass at time *t.* The expression $\left|\vec{r}_i(t) - \vec{r}_i(0)\right|^2$ is known as the mean square displacement. The mean square displacement can be found by comparing the position of the water molecules at any time after the start of a simulation. The crossing of periodic boundaries must be included in position calculations, lest the dimensions of the simulation box limit the mean square displacement.

## 2.5 Designation of Molecules as Liquid-like or Solid-like

The solid-liquid interface cannot be characterized without recognizing where the solid phase ends and the liquid phase begins. Bulk properties cannot be applied, as the interface is nanoscopically thin (typically around 10 Å). Individual molecules must be defined as occupying liquid-like or solid-like environments. A molecule's relationship with its nearest neighboring molecules can provide methods to determine a molecule's identity, as belonging to the liquid or the solid phase.

An established solid-liquid criterion is an angular order parameter developed for silicon by Uttormark [39] and modified for water by Báez [40]. It involves both the identification of the nearest neighbors and the angles of the oxygen-oxygen bonds formed by the nearest neighbors with the molecule in question.

The first parameter necessary to use the Báez criterion is the maximum distance at which two molecules can be considered nearest neighbors. A convenient coordinate for the molecule-molecule separation distance is that of the oxygen atom. The oxygen-oxygen radial distribution pattern for TIP4P-FQ liquid water has already been found by Rick [14] and is shown in Figure 2.4. The first local minimum represents the cutoff distance for the first nearest neighbor, which for TIP4P-FQ water occurs at about 3.3 Å. Integration of the radial distribution function, $g_{OO}(r)$, over this

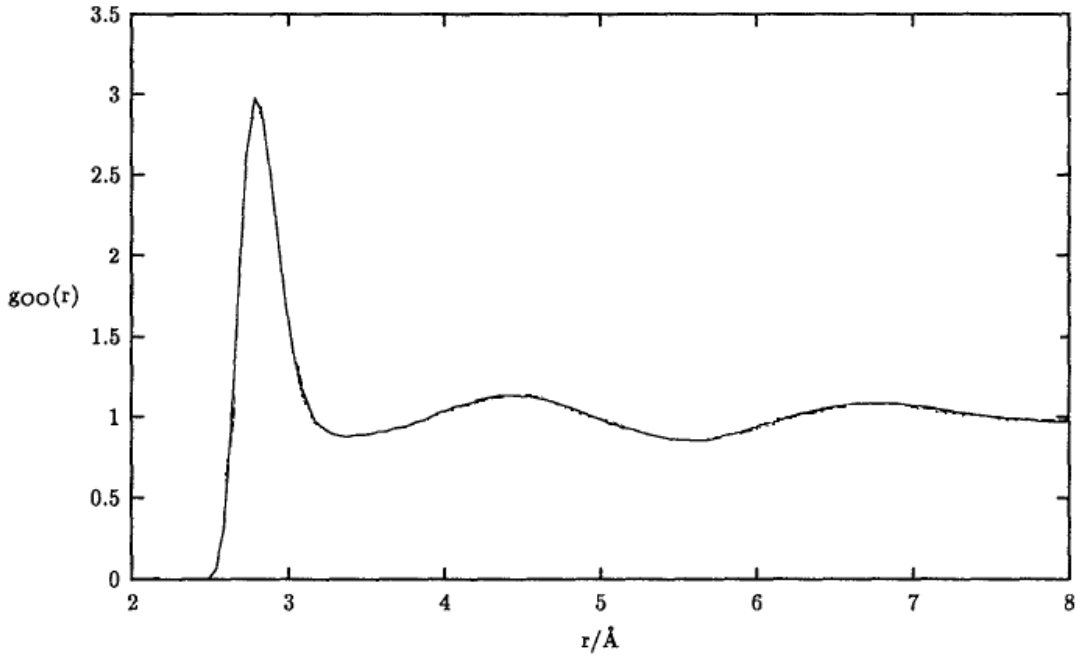


Figure 2.4. Oxygen-oxygen radial distribution function for the TIP4P-FQ water potential. Source: [14]

distance gives 4.4 nearest neighbors for liquid water, which agrees with experiments using neutron diffraction [41]. Ice has four nearest neighbors and a cutoff distance of about 3.5 Å. Because of the similarities in maximum number and cutoff distances for nearest neighbors, identification of nearest neighbors alone is insufficient to differentiate solid from liquid water. Using the tetrahedral structure of ice is a common strategy.

Ice has a tetrahedral structure. For an ideal lattice, the angle formed between the oxygen atom of a water molecule and the oxygen molecule of two of its nearest neighbors should be 109.47°. The water molecule can expand its hydrogen-oxygen-hydrogen bond angle from about 106° to accommodate this. While the HOH angle in the TIP4P-FQ water molecule is fixed at 104.52°, it can still form a tetrahedral-like structure. Therefore, an angular order parameter, $F_w$, can measure the deviation from perfect tetrahedral bonding of 109.47° as

$$F_w = \sum_{i=1}^{N} \left( \left| \cos(\varphi_i) \right| \cos(\varphi_i) + 1/9 \right)^2 , \tag{2.19}$$

where $\varphi_i$ is the angle formed by the oxygen atom of the molecule with the oxygen atoms of any two nearest neighbors, and N is the number of distinct angles that can be formed with any pair of nearest neighbors. For a water molecule with a full complement of nearest neighbors, $N = {}_4C_2 = 6$. A molecule may have fewer neighbors because it is adjacent to a vacancy or is located at a solid-liquid interface; N would be 3 and 1 for 3 and 2 nearest neighbors, respectively. $F_w$ is zero for an ideal lattice and has positive values for all other configurations. A water molecule is considered ice-like if $F_w$ is less 0.4.

This method distinguishes solid from liquid with a high degree of accuracy. However, the parameter cannot distinguish between many ice types, as cubic ice, ice-seven, -eight, -ten, and -eleven all have oxygen-oxygen bond angles of 109.47, and several other ices possess a range of angles with $F_w < 0.4$.

## 2.6 Interfacial Growth

At temperatures above the melting point, the Gibbs free energy of liquid water is lower than that of ice, and the solid-liquid interface recedes. The higher the temperature, the greater the driving force and the kinetic energy of individual molecules, and the interface recedes at a high velocity. At temperatures below the melting point, the opposite occurs: the free energy of fusion increases, encouraging ice growth. However, the kinetic energy of the molecule decreases as well, slowing the assembly of ice crystal and overall crystal growth. At very low temperatures, the low kinetic energy becomes the limiting factor, halting crystal growth along the interface and forming a glass instead. At a certain temperature below the melting point, the interface is growing at its maximum velocity; below this temperature kinetic energy is rate-limiting, and above it the free energy of fusion is rate-limiting.

While the solid-liquid interfaces of all ice surfaces are stable at the melting point, the rate of growth of the interfaces is different at the same temperature. Ice grows slowly from the basal interface (S1 ice) and quickly along the prismatic interface (S2 ice). Prismatic growth requires the positioning of only two water molecules on the interface to complete a hexagonal ring, thereby reclassifying themselves as solid molecules, while basal growth requires three water molecules, causing the anisotropy.

This study is concerned with the kinetics of ice crystallization and a characterization of the prismatic ice-water interface. As seen in Figure 2.5, the prism $\{10\bar{1}0\}$ faces are made up of parallel hydrogen bonds lying in the (0001) direction, also known as the c-axis.

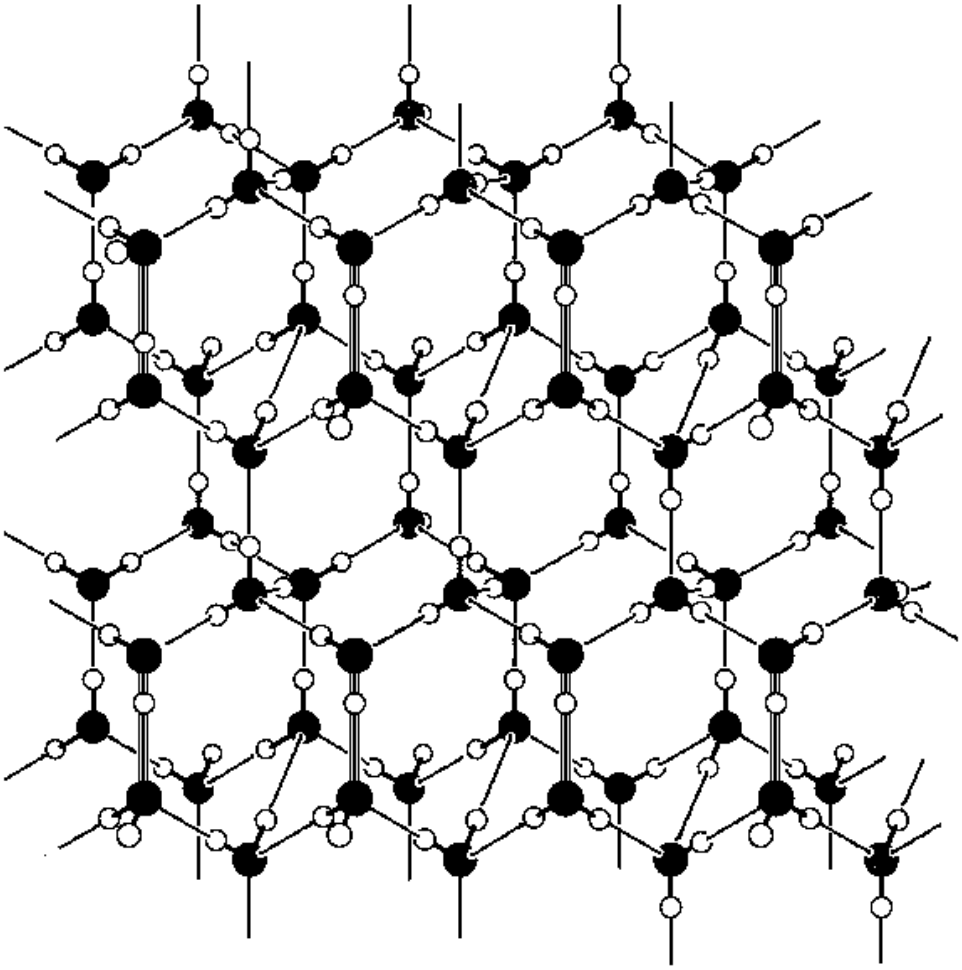

Figure 2.5. Prismatic surface of hexagonal ice, shown by vertical striped bonds. Oxygen atoms are black, hydrogen atoms are white.

Measurement of interfacial growth on the solid-liquid interface has been difficult, in part due to the challenges involved in undercooling liquid water below its freezing point. Hallett [42] measured growth on the prism interface of ice from water supercooled by 1-20 K, and found an empirical relation for V, the velocity of ice growth, and the undercooling, $T_s$:

$$V = (0.0008 \pm 0.0001) T_s^{(1.9 \pm 0.05)} \tag{2.20}$$

which results in a maximum speed of 1.2 m/s at 20 K of undercooling. The incredibly small dimensions and fast movement of the solid-liquid interface makes characterization by experiment a near impossibility, and can only be performed by molecular simulation.

### 2.6.1 Interfacial Motion as a Measurement of Melting Point

Derivation of the melting point of a molecular model is typically performed by calculation of the Gibbs free energy [43]. Thermodynamic integration [44] is used to calculate the free energy difference between the model system and an ideal system with known energy. This method has been used for several popular models, some of which are shown in Table 2.2.

However, two other techniques can be used to directly calculate the melting point temperature: two-phase coexistence and interface motion. Both examine the interactions within a two-phase system.

The two-phase coexistence method involves the relaxation of a two-phase system to equilibrium. The two phases are separately prepared. For a solid-liquid system, the solid phase is typically equilibrated at a temperature below the suspected

melting temperature using the isobaric-isothermal (NPT) ensemble. The liquid phase is melted from a copy of the solid phase using the isochoric-isothermal (NVT) ensemble, then cooled to a temperature above the suspected melting point. The two phases are put into contact at a particular solid surface, and further relaxed in the NPT ensemble to reduce interfacial contact stress. The system is then equilibrated in the isobaric-isoenthalpic (NPH) ensemble, until the instantaneous kinetic temperatures of both the solid and liquid phases are equal. This method has been applied both to silicon [48] and to water [46].

Table 2.2. Melting temperatures ($T_m$) of common water models, as determined by different methods.

| Model | $T_m$ | Method | Reference |
|---|---|---|---|
| SPC/E | 225 ± 7 K | Free Energy | [33] |
| | 225 ± 5 K | Interface Motion | [23] |
| TIP4P | 238 ± 6 K | Free Energy | [45] |
| | 229.3 ± 1.0K | 2 Phase Coexist | [46] |
| TIP4P-Ew | 245.5 K | Free Energy | [33] |
| | 257.0 ± 1.1K | 2 Phase Coexist | [46] |
| TIP5P | 268 ± 6 K | Free Energy | [47] |
| | 272.2 ± 0.6 K | 2 Phase Coexist | [46] |
| TIP6P | 271 ± 9 K | Free Energy | [29] |
| | 280 – 285 K | Interface Motion | [9] |

Interface motion is a nonequilibrium method that relies on the movement of the solid-liquid interface to determine the melting point. It is performed in the NPT ensemble. The interface is identified by changing the ratio of solid and liquid

molecules along the length of the simulation box normal to the interface. A particular ratio can be selected along the interface, and its position tracked at a given temperature. Simulations are run at different temperatures, and the melting point is found by eliminating those systems that exhibit definite interfacial movement.

The most common models were not parameterized to simulate an accurate melting temperature, and no model has been specifically subjected to all three melting point determination methods. However, there is a good comparison when two of the methods are used, usually with different system sizes. (Table 2.2) This suggests that while unconventional, interfacial movement can not only describe interface characteristics and crystallization kinetics, but also supply a robust measure of the melting point.

### 2.6.2 Previous Simulation Results

Most interface studies of water have focused on stability, as interfacial growth is long relative to ordinary simulation time. Only recently has computational power allowed an effective analysis of interfacial growth for water whereas the interfacial response function is well known for silicon [49] and germanium [50].

The first simulation of the ice-water interface was performed by Karim and Haymet [20]. Using the TIP4P model, a liquid-solid-liquid system of 1440 molecules with basal interface was measured for average properties over a 52.8 ps interval at 240 K. They identified that liquid far from the interface retains the characteristics of bulk liquid, and declared a broad interface of about 15 Å. The diffusion constant in the interfacial region lies between those of the liquid and the solid.

Anisotropic interface properties were quickly identified: the orientation of the ice crystal and the ice molecules on the surface has a dramatic effect on the properties of the interface. The basal interface is thinner than the prismatic interface, and the prismatic interface is more geometrically "rough" and exerts a greater influence over the translational order of molecules in the interface [21]. Higher index faces, such as the secondary prism $\{2\bar{1}\bar{1}0\}$ and the pyramidal $\{2\,0\bar{2}\bar{1}\}$ planes have even smoother interfaces [22]. Surface melting studies on the different ice orientations reveal different characteristics of the quasi-liquid layer that forms at temperatures near the melting point of water. The prismatic surface has a much larger temperature interval for the transitional state between a molecularly flat surface and active surface melting; the basal surface has a larger quasi-liquid layer [51]. Self-diffusion and vibrational motion is greater for the basal surface, due to the relative independence of the dangling O-H bonds from the hydrogen bond network of the solid [52].

The growth kinetics of the solid-liquid interface of water were first approached by Nada and Furukawa [53]. The growth mechanisms for the basal and prismatic interfaces are very different. Basal growth occurs one layer at a time; each new layer is nearly complete before construction of a new layer begins. This layer-by-layer approach is consistent with the thin interface established by equilibrium simulations. Prismatic growth from the thick, rough interface can be characterized by a collected molecule process: water molecules in the region collectively form the ice crystal structure. Each crystallized prism layer is far from complete when a new prism layer begins formation. Translational order develops before orientational order in both systems [54]. While the kinetics of growth differ, the melting point for both interfaces is the same, though the basal surface displays greater stability [23].

Nada and Furukawa also developed data for the velocity as a function of temperature using the TIP6P model, collecting information that can be used to construct part of the interface response function for water [9]. Seven velocities were calculated for temperature interval between 268 K and 287 K (Figure 2.6). While this data establishes a melting point in the range 280 K–285 K, the 17 K temperature interval limits complete characterization of the growth kinetics for greater subcooling.

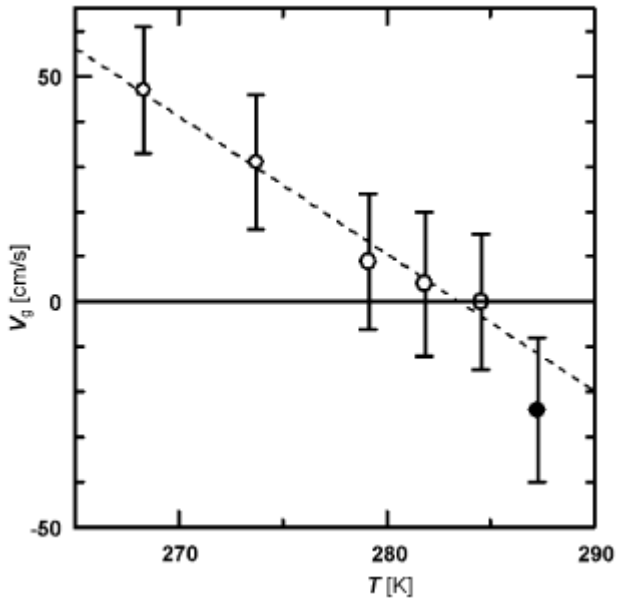


Figure 2.6. Interface motion for the TIP6P water model between 270K and 287K. Source: [9]

### 2.6.3 Wilson-Frenkel Equation

The movement of an interface separating the crystalline and liquid phases can be written in terms of rates of adsorption and desorption to an interface, as in the Wilson-Frenkel equation:

$$V = \lambda \omega_o \exp\left(-\frac{\Delta G_{mL}}{kT}\right)\left[1-\exp\left(\frac{\Delta G_f(T)}{kT}\right)\right] \tag{2.21}$$

where $\lambda$ is the jump distance, $\omega_o$ is the vibration frequency, $\Delta G_f$ is the free energy of fusion, $\Delta G_{mL}$ is the energy required to move from positions of minimum energy in the liquid phase, and T is the temperature. The first exponential reflects the growth of the interface due to adsorptive events, while the second exponential term captures desorption events. Measuring the change in the separation distance between the two defined interface points allows the average interface velocity to be determined.

# Chapter 3

# Prismatic Growth and Melting

This chapter describes the movement of the solid-liquid interface of an ice-water system followed for 500 to 750 picoseconds at a range of temperatures from 265 K to 310 K, which was expected to bridge the melting transition. Location of the interface and the measurement of its movement are found by a determination of local order within an interval, or "slice," of the system. Interface growth and melting are analyzed in terms of changes in local system ordering and from density and dipole profiles. The concurrent growth development of two prismatic layers at the interface suggests three-dimensional growth, as opposed to a layer-by-layer method, which matches Nada and Furukawa's findings using the TIP6P model [9]. The melting temperature of TIP4P-FQ is found to be 303 ± 8 K, and the maximum interface velocity is estimated to be about 1 m/s. We show that a Gibbs-Duhem integration for a reparameterized TIP4P-FQ model predicts a melting point of 276 K; the interface response of the ice-water-ice system using this modified model supports that prediction.

## 3.1 Set-up

The initial configuration described in section 2.3 was simulated at several temperatures to determine the interface response function introduced in section 2.6. Simulations were performed using the isobaric-isothermal (NPT) ensemble by coupling the system to a pressure bath and a Nosé-Hoover thermostat [24].

Simulations were carried out at temperatures from 265 K to 310 K, at intervals of 5 K. Each simulation was run for 0.5 ns; runs in the interval 285 K to 300 K were simulated for 0.75 ns to better discern movement of the interface as a function of time. The fluctuating charges were propagated using the extended Lagrangian technique and the simulations used a 1 fs time step. The simulation was sampled every 50 ps for the first 100 ps, and 25 ps thereafter. The coordinates of the oxygen and hydrogen atoms were recorded to determine order along the length of the simulation box. Atom location and charges on the hydrogen and M-sites were averaged over the length of each time interval to provide smoothed density and dipole profiles.

## 3.2 Self-Diffusivity

Comparison of the diffusion constant of the TIP4P-FQ model used here to that found by Rick [18] confirms the quantitative accuracy of our application of the TIP4P-FQ model, as well as allowing us to infer that the model is resilient to changes in the size of the simulation box. The simulation used by Rick contained 256 water molecules, while this simulation is over four times as large with a different geometry. This simulation also contains hexagonal ice and, while only liquid diffusivity is being investigated here, its robustness in a heterogeneous environment will also be tested. The self-diffusivity should match that in the original simulation, and it is found that the results here vary from the results in Rick [18] by no more than 15%.

### 3.2.1 Sampling Method

As only the diffusion constant of the liquid phase is of interest, it is important to isolate a section of the simulation box that remains liquid. At all temperatures simulated, a 10 Å wide slice along the length of the box in the middle of the simulation remains in the liquid phase, well away from the solid-liquid interface. Measuring the diffusivity of water molecules whose trajectories begin and end only in this slice assures that the water molecules measured remained in the liquid phase for the duration of its trajectories. In the time intervals measured, it would be extraordinarily rare for a water molecule to leave the observed slice, join and break away from the interface, and return to the slice.

At all temperatures studied, sampling began 100 ps after the start of the simulation. The location of the water molecules was based on the coordinates of their oxygen atoms. Net distance traveled by the oxygen atoms was measured every 25 ps. Diffusivity was measured using the Einstein relation (equation 2.18).

### 3.2.2 Coefficient Comparison

A comparison of the self-diffusivity calculated here compared to those found by Rick finds the data to be nearly indistinguishable, as seen in Figure 3.1. The diffusivities found by Rick lie well within the first standard deviation error bars, and typically differ by less than 5% and no more than 15%.

When fitted to the empirical relation $D = D_o T^{1/2}\left(T/T_S - 1\right)^{\gamma}$, the parameters are $D_o = 0.199$ A$^2$/ps, $T_S = 229$ K, and $\gamma = 2.37$, compared to Rick's values of $D_o = 0.115$ A$^2$/ps, $T_S = 250$ K, and $\gamma = 1.42$, and experimentally derived values of

$D_o = 0.087$ A$^2$/ps, $T_S = 220$ K, and $\gamma = 1.81$. Parameter differences between these results and Rick's results can be attributed to the restriction in the lengthwise direction by the slice used to select water trajectories, and to the sensitivity of the relation to small changes. Overall, these results support the use of the TIP4P-FQ model for further simulations.

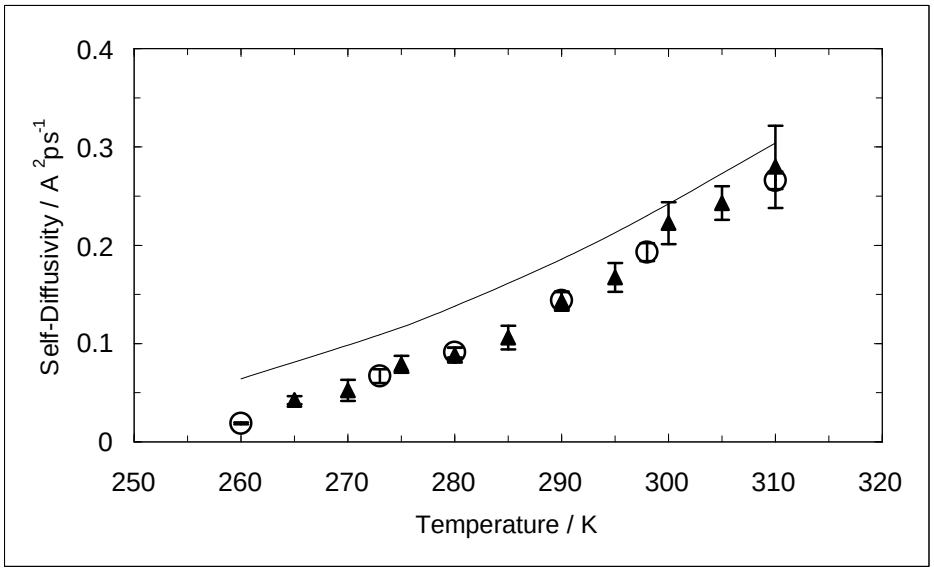


Figure 3.1. Self-Diffusivity of the TIP4P-FQ water model as determined by Rick [18] (circles) and by this researcher (solid triangles), and compared to experiment [55,56] (solid line).

## 3.3 Interface Response Function

The interface response function charts the movement of a solid-liquid interface by crystallization and by melting. A positive velocity is associated with a crystallizing interface, and a negative velocity is associated with a melting interface.

The interface response function in this simulation was measured here by observation of the two solid-liquid interfaces existing in the ice-water-ice set-up.

From that observation, the melting point and maximum crystallization velocity can be determined. Interface velocity can also be used to compare the original TIP4P-FQ model to a modified version.

### 3.3.1 Sampling Method

At each sampling, all the water molecules in the simulation box were determined to have either solid-like or liquid-like characteristics based on the Báez angular criterion described in Section 2.5. While this criterion can classify individual molecules, solid and liquid phases are characterized by the overall qualities of large groups of molecules. Bulk classification can be accomplished by a tray method that divides a simulation into many slices. The slices are then characterized as liquid-like or solid-like by an order parameter defined as the percentage of solid-like water molecules in each slice. Solid-like phases typically have greater than 90% order, while liquid-like phases have less than 10% order.

Figure 3.2 illustrates this method for the initial configuration of the simulation. The bulk solid phases and the bulk liquid phase are clearly evident, but classifying the interfacial region by eye is difficult. Thus to identify the interfacial region, we begin by dividing the simulation box lengthwise into 3 Å wide slices. Each slice contains about 30 to 60 water molecules, which we have found by experience to be an adequate number to characterize the composition of each slice. The order of each slice is then determined by the ratio of "solid-like" molecules to total molecules in the slice. A complete tetrahedral structure has an order value of one, while a random distribution of molecules would have an order value close to zero.

The solid phases, solid-liquid interfaces, and liquid phases are evident in Figure 3.2. The solid phase is not always a perfect, defect-free solid, and the liquid phase shows some transient order. Existence of liquid-like molecules in the solid phase and solid-like molecules in the liquid phase can be attributed to thermodynamic fluctuations and short-term water clustering, respectively. We find that the interfaces that separate the phases are about 5-6 Å wide. The order in these interfaces gradually moves from solid-like to liquid-like.

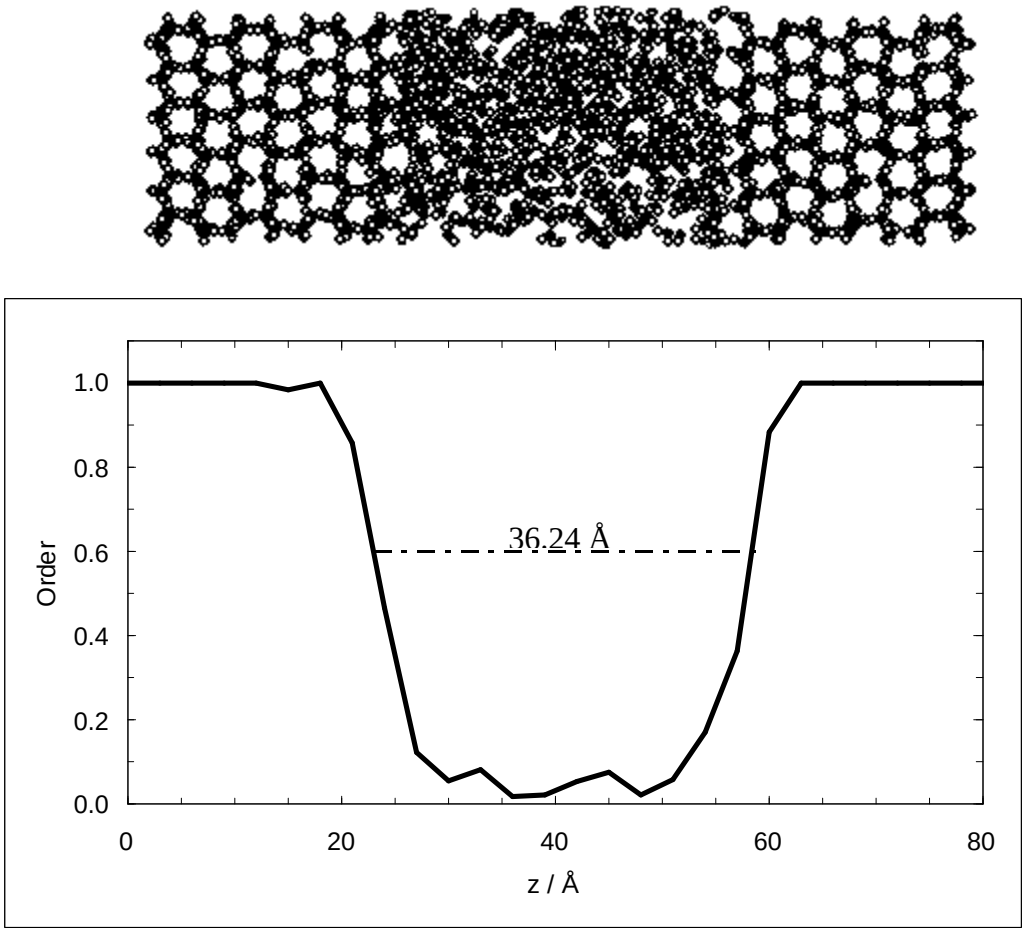


Figure 3.2. Order profile of initial ice-water-ice configuration as measured from the left-hand side of the box. A perfectly tetrahedral structure has an order of one; liquid has an order less than 0.1. The assigned distance between the interfaces is 36.24 Å.

Interface movement can be determined by measuring the distance between the two interfaces. During periods of crystallization, the two interfaces will move closer together and the distance between them will decrease. When the simulation is undergoing melting, the two interfaces move further away from each other, increasing the distance. By arbitrarily locating the interface where the order is 0.6, the distance between the interfaces can be consistently measured. This location is well within the interface interval, and is clearly neither solid-like nor liquid-like. For the initial configuration, the distance between the 60% order locations on the two interfaces is 36.24 Å. Note that that the speed of the moving interface could have been determined by following any appropriate reference point in the interfacial region.

### 3.3.2 Interface Response Function and Melting Temperature

By measuring the change in distance between the two interfaces over a given time interval, an average crystallization velocity can be found. By convention, the velocity is positive for crystal growth, and negative for melting. When the velocity is zero at non-zero temperatures, the interfaces have zero net movement and the system is at the melting point: adsorption and desorption events along the interface occur at equal rates.

Figure 3.3 shows the distance between interfaces over time for a few of the temperatures simulated. At 310 K, the ice phase is clearly melting as the distance between the two interfaces grows. At 295 K and 280 K, the distance between the interfaces is shrinking as crystallization is occurring. Note how much faster interfacial growth is at 280 K in comparison to 295 K; the kinetics of crystallization are faster at

280 K than they are at 295 K. At 300 K the interface is relatively stable, and thus this temperature should be very close to the melting temperature of the TIP4P-FQ model.

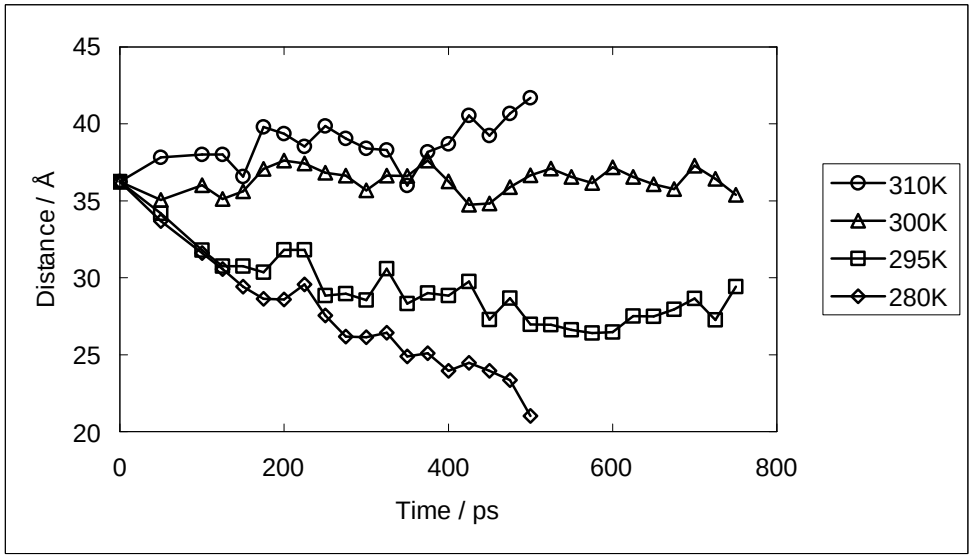


Figure 3.3. Distance between the two interfaces during simulations at selected temperatures. Decreasing distances correspond to ice growth and increasing distances to melting.

The change in the interface distances over time is the combined velocity of the two interfaces. Halving this velocity gives the average kinetics of crystallization for a single solid-liquid interface. When organized according to temperature, the result is the interface response function (Figure 3.4). Velocity is determined by least squares regression. Error bars represent one standard deviation.

The melting temperature occurs at the temperature where the interface response function is zero. Based on the 95% confidence interval using the standard deviation of each velocity, the interface response at 300 K and 305 K cannot be distinguished from zero velocity, whereas the interfaces at all other temperatures are

definitely either melting or crystallizing. Therefore, the melting temperature of TIP4P-FQ should lie within five degrees between 300 K and 305 K.

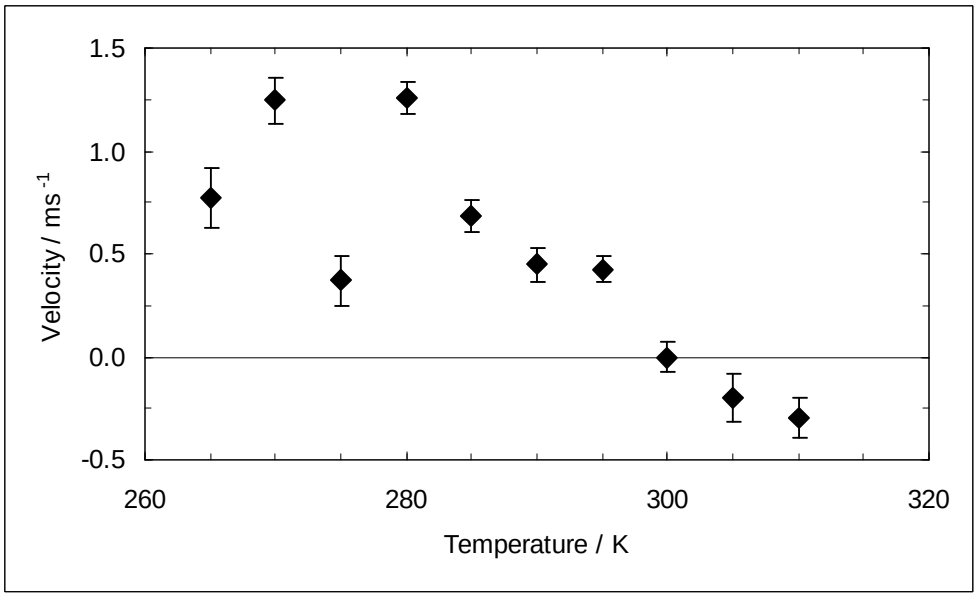


Figure 3.4. Average velocity of ice-liquid interface at temperatures between 265 K and 310 K.

Note also in Figure 3.4 how the interface response function steadily decreases at temperatures above 280 K. At temperatures below 285 K, the velocities are erratic and suggest a downward trend. The kinetic energy of liquid molecules is decreased such that the rate of adsorption events slows relative to the rate of desorption events. This behavior is expected: at lower temperatures, the liquid regions should eventually become glass-like, effectively halting interface growth.

### 3.3.3 Wilson-Frenkel and Maximum Interface Velocity

The Wilson-Frenkel equation (section 2.6.3) can be applied to the interface response function to better characterize the kinetics of crystallization. Known parameters from

experimental data for water were used as initial parameters, and a non-linear optimization program was used to modify the values to the interface response function of the TIP4P-FQ water model. Both $\Delta G_{mL}$ and the entropy, used to determine the free energy of fusion, were assumed to be constant over the temperature range. For the least squares fit, $\Delta G_{mL}$=12.123 kJ/mol and $\Delta G_f$=7003.8 – 23.120 T(K) J/mol.

The Wilson-Frenkel equation is displayed with the known velocities in Figure 3.5. The temperature at which the velocity is zero, namely the equilibrium melting point, as determined using the Wilson-Frenkel equation is found to be 303 K. This value lies between the two temperatures whose interfaces could not be discounted as having zero velocity, 300 K and 305 K. Supported by the fact that the systems at 295 K and 310 K clearly freeze and melt, respectively, the melting temperature can safely be described by the IRF-derived value of 303 ± 8 K.

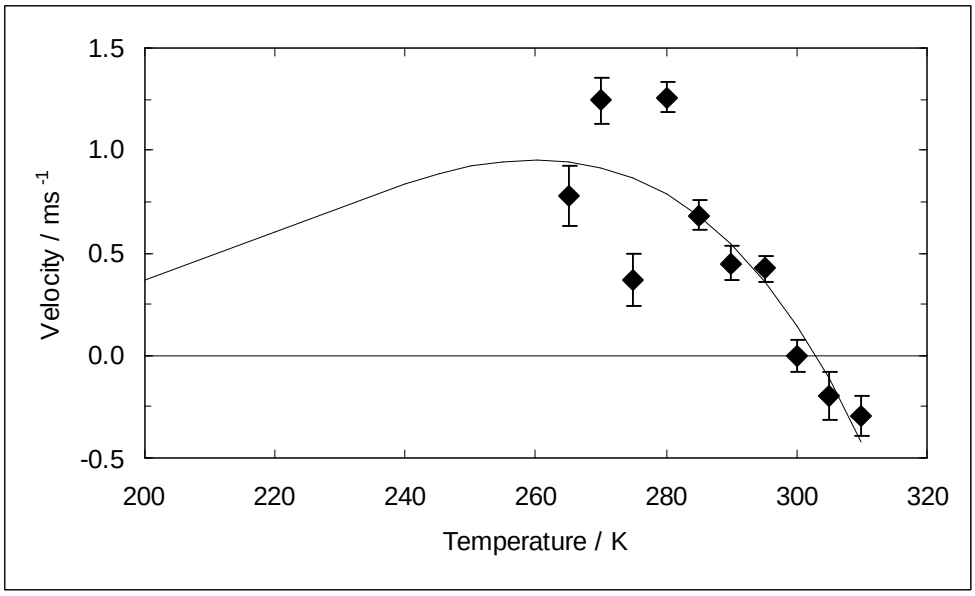


Figure 3.5. Interface response function for TIP4P-FQ ice $I_h$. Wilson-Frenkel curve (Equation 2.21) fitted using a least squares fit (solid line).

For increasing undercooling, the driving force provided by the free energy of fusion increases, but the kinetic energy of the molecules decreases. Initially, the solid will grow faster as the undercooling increases but, at some point, the interface growth will decelerate as the water molecules move more slowly into position in the crystal lattice of the ice, giving rise to a maximum interface velocity. The Wilson-Frenkel equation fitted to our data suggests that a maximum interface growth of around 1 m/s occurs at 260 K, an undercooling of around 40 K. This is about an order of magnitude slower than silicon or germanium [49,50], and two orders of magnitude slower than sodium [19]. The velocities fluctuate significantly from the Wilson-Frenkel equation at temperatures lower than 285 K and, given the absence of simulation data at temperatures below 265 K, it is unlikely that the quantitative accuracy of the prediction of the maximum growth velocity can be adequately assessed.

### 3.3.4 Melting Point for a Modified TIP4P-FQ Model

A modified version of the TIP4P-FQ model has also been made by Rick [18] to correct for an ice phase density that is too large using the original model. The $\sigma$ parameter of Lennard-Jones interaction was increased from 3.159 to 3.173 Å, leaving all other parameters unchanged. This results in a solid density of 0.921 g/cm$^3$, compared to an experimental value of 0.917 g/cm$^3$, as well as an improved heat of sublimation compared to the original model. $\Delta H_{sub}$ changes from 13.39 to 12.56 kcal/mol, compared to an experimental value of 12.20 kcal/mol [57].

The melting temperature of the modified model has been calculated using a Gibbs-Duhem integration method described by Kofke [58]. For small parameter

changes, such as the one made for the modified TIP4P-FQ model, the modified melting temperature can be estimated at the new value from

$$T_m(\sigma_2) = T_m(\sigma_1) + \left(\frac{\partial T}{\partial \sigma}\right)_{\sigma=\sigma_1} (\sigma_2 - \sigma_1) \tag{3.1}$$

where

$$\left(\frac{\partial T}{\partial \sigma}\right)_{\sigma=\sigma_1} = \frac{T(\lambda_{\sigma S} - \lambda_{\sigma L})}{h_S - h_L} \tag{3.2}$$

$\mathbf{h}_\alpha$ is the enthalpy of the α phase divided by N, the number of molecules in the simulation, and

$$\lambda_{\sigma\alpha} = \frac{1}{N}\left(\frac{\partial G}{\partial \sigma}\right) = \frac{1}{N}\left\langle\left(\frac{\partial U}{\partial \sigma}\right)\right\rangle = \frac{1}{N}\left\langle \sum_{i<j} \frac{24\varepsilon}{\sigma}\left[2\left(\frac{\sigma}{r_{ij}}\right)^{12} - \left(\frac{\sigma}{r_{ij}}\right)^{6}\right]\right\rangle \tag{3.3}$$

which was evaluated for the solid and liquid phase by Sturgeon and Laird [59]. Using this method, the melting temperature of the modified TIP4P-FQ model has been found to be 276 K [60].

Confirmation of this estimate can be made by observing the movement of the interfaces in the ice-water-ice simulation using the modified parameters. The same initial configuration was used as in the original simulations. The system was simulated at 276 K, to verify zero net movement of the interface, and also at 285 K, to ensure that melting occurs at temperatures above the melting point. The simulation lasted for 500 ps, and the interface positions were evaluated after the first 50 ps and 100 ps and every 25 ps thereafter.

The different characteristics of the modified model can be exemplified by comparison at analogous temperatures. (Figure 3.6) At 275 K, the original model clearly shows crystal growth, while at 276 K, the modified model shows little interface movement. The modified model also melts at 285 K; the original model has demonstrated freezing at that temperature.

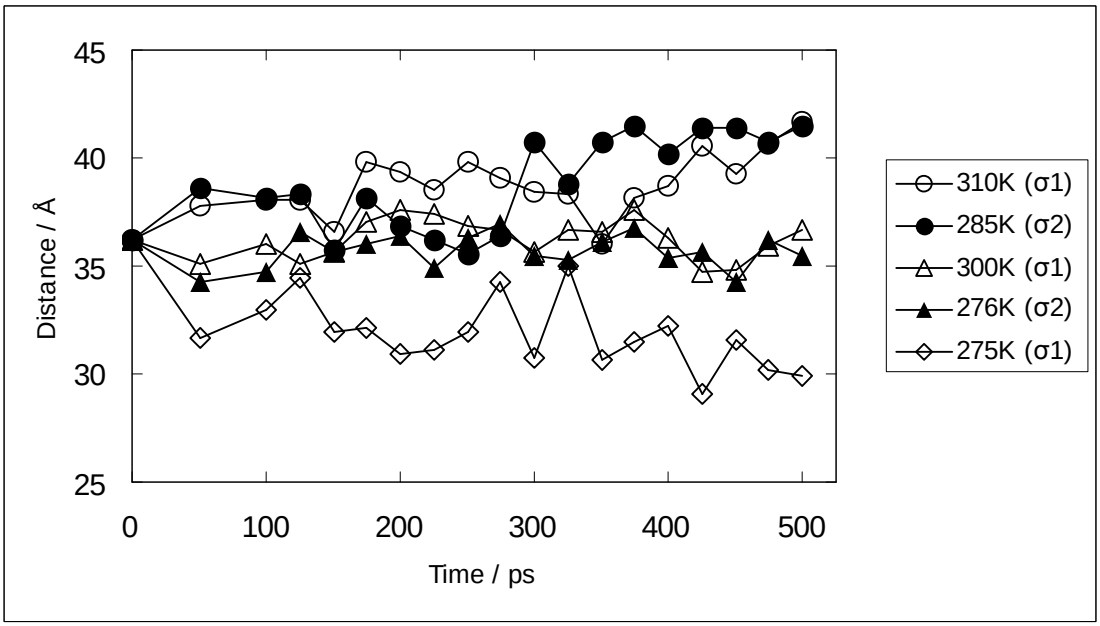


Figure 3.6 Distance between the two interfaces during simulation for Lennard-Jones parameters $\sigma_1$=3.159Å (original parameter set [14]) and $\sigma_2$=3.173Å (modified parameter set [18]).

The interface movement of the modified model can be compared to that of the original TIP4P-FQ model relative to their respective melting temperatures. (Table 3.1) At 276 K, the interface movement of the modified model is similar to that of the original model at 300 K, and near to the original model's melting point. The fluctuations of these two simulations are also similar, as standard deviations of the interface movement are within 14% of each other. The small movement at 276 K

velocity; 276 K is thus an excellent estimate for the melting temperature of the modified TIP4P-FQ model.

Table 3.1. Average velocity slopes of the ice-water interfaces, standard error of the velocities, and the probability of zero average movement of the interface for Lennard-Jones parameters $\sigma_1$=3.159Å (original parameter set [14]) and $\sigma_2$=3.173Å (modified parameter set [18]).

| | $T_m$ + ~10K | | ~$T_m$ | | |
|---|---|---|---|---|---|
| Temperature (K), σ | 310, $\sigma_1$ | 285, $\sigma_2$ | 300, $\sigma_1$ | 276, $\sigma_2$ | 275, $\sigma_1$ |
| Slope (m/s) | -0.299 | -0.527 | -0.003 | -0.004 | 0.369 |
| SE(Slope) | 0.099 | 0.135 | 0.074 | 0.065 | 0.123 |
| P(\|slope\| not> 0) | 0.0069 | 0.0011 | 0.972 | 0.995 | 0.0075 |

At temperatures greater than five and less than ten degrees above the calculated melting point, the interfaces clearly melt. At 285 K, the equivalent of $T_m$ + 9 K, melting occurs faster for the modified model than for the original model at 310 K, the equivalent of $T_m$ + 7 K. While the complete interface response function is unknown for the modified TIP4P-FQ model, the relative speeds support the estimate of 276 K as the melting temperature for the modified model.

## 3.4 Density Profile

Density is the ratio of mass to unit volume. The density of TIP4P-FQ in both the liquid and solid phase has been investigated by Rick [18]. TIP4P-FQ has a temperature of maximum density at 280 K, close to the experimental value of 277.13 K. The density of liquid TIP4P-FQ is well established between 260 K and

310K, and the density of TIP4P-FQ ice is known at 273 K. While this is useful in identification of bulk phases, examination of density along small length intervals can describe interface characteristics and the crystalline growth mechanism.

### 3.4.1 Identification of Solid and Liquid Phases

To characterize the density along a stable solid-liquid interface, an interval of time was chosen that showed zero net movement at a temperature near the established melting temperature. The interface between 325 ps and 350 ps at 300 K falls within these requirements (Figure 3.3). In this interval, the distance between the interfaces decreases from 36.642 Å to 36.609 Å, a change of 0.09%. Local density was calculated every 0.05 Å and averaged for the duration of the simulated time interval, 25 ps.

The density profile parallel to the prism interface with liquid water is seen in Figure 3.7. The bimodal peaks on the left of 27 Å characterize the double molecular layers typical of the prismatic face of ice, while the rough values hovering near 1 g/cm$^3$ to the right of 33 Å is definitely liquid. Peak heights in greater proximity to the interface have lower values than those peaks deeper in the ice bulk. The area between 27 Å and 33 Å sees a gradual deconstruction of crystalline order to the randomness of the liquid state. This 6 Å wide interface is in agreement with the interface characterization made by order determination (Figure 3.2). It also shows that the interface involves two prismatic layers: a solid-like layer between 27 Å and 30 Å, and liquid-like layer between 30 Å and 33 Å.

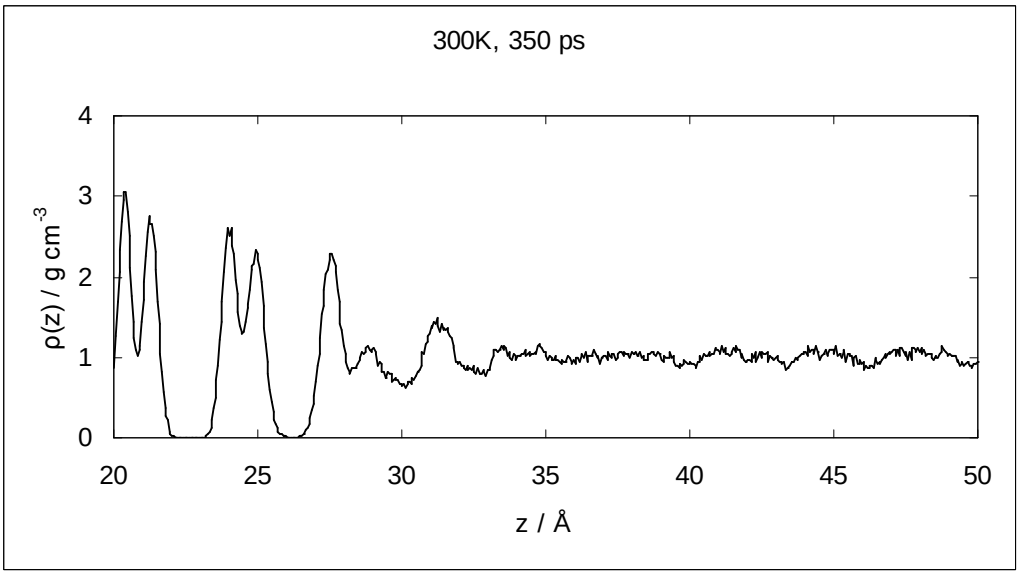


Figure 3.7. Density profile of a stable interface along the length of the model after 350 ps of simulation at 300K, averaged over the previous 25 ps.

### 3.4.2 Change in Density Profile with Growth

Observation of the density profile during interface growth over time suggests that crystallization is a two-layer process. For example, very fast crystal growth occurred at 280 K, and the time intervals averaged at 300 ps, 400 ps, and 500 ps display complete growth of a prismatic layer (Figure 3.8).

Crystalline and interfacial growth can be observed using the density peaks centered about 32 Å, 35 Å and 38 Å. At 300 ps, the 32 Å pair of peaks is clearly solid-like (section A in Figure 3.8), but the disparity in peak height places it within the interface. The 35 Å peak (section B) is not bimodal, and is the liquid-like layer in the interface; no peak near 38 Å (section C) is discernable from natural density variations in the liquid phase.

At 400 ps, the peak heights of the bimodal layer in section A is now characteristic of a solid phase ice layer near the interface; it has left the interface and joined the solid phase. The section B peak in the interface has moved from liquid-like to solid-like by evolving from a single peak to a bimodal one. Meanwhile, a definite single peak is present in section C. Between 300 ps and 400 ps, the two ice-layer wide interface has shifted over one layer.

The density profile at 500 ps illustrates a more defined interface. The left peak of the section B layer has increased in height, signifying that it is becoming more ice-like. The peak in section C has narrowed as it becomes less liquid-like. A local maximum at 41 Å where one has never been in the previous two profiles suggest the section B layer at 38 Å is developing a bimodal peak. Between 400 ps and 500 ps, the interface has not moved over one complete ice layer as it did between 300 ps and 400 ps, but is rather solidifying development of the two layers involved in the interface point towards a moving interface.

Figure 3.8. Density profile of a growing interface along the length of the model after 300, 400 and 500 ps of simulation at 280 K, averaged over the previous 25 ps.

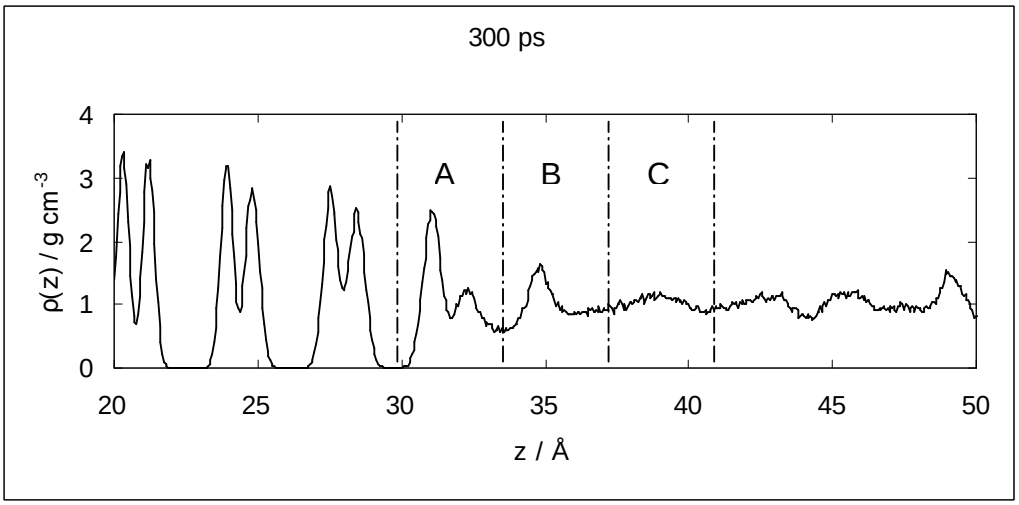
300 ps
ρ(z) / g cm-3
z / Å
A
B
C

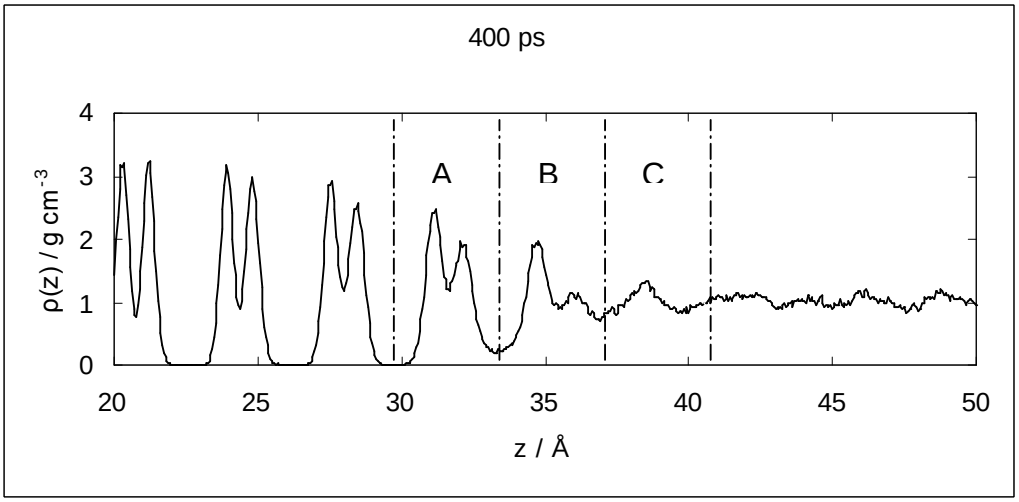
400 ps
ρ(z) / g cm-3
z / Å
A
B
C

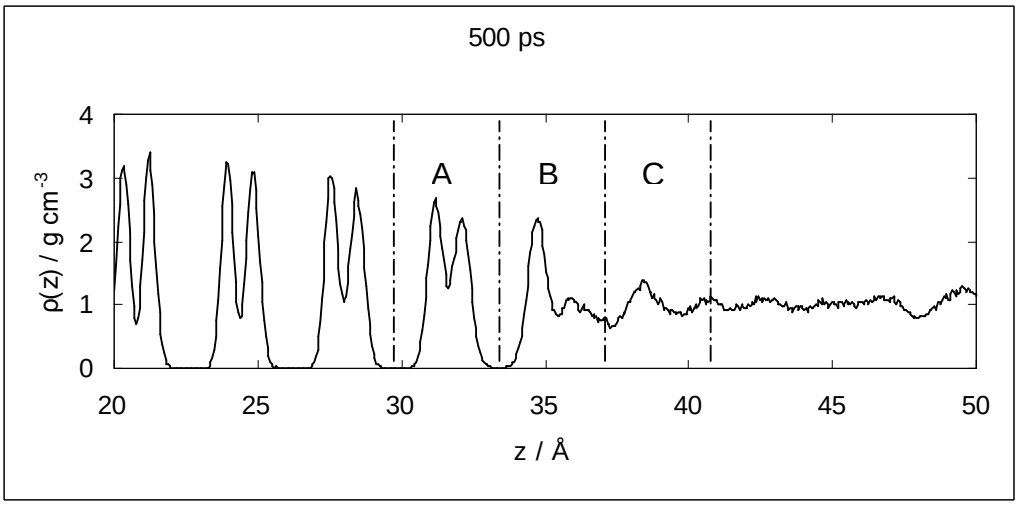
500 ps
ρ(z) / g cm-3
z / Å
A
B
C

## 3.5 Dipole Profile

The dipole moment occurs as the result of the uneven distribution of opposite charges. It is the product of the charge magnitude and the distance between the two charges. While the TIP4P-FQ water model has no net charge, the fluctuating negative charge at the M-site and the positive charges at the hydrogen site produce a net dipole moment bisecting the HOH angle in the direction of the oxygen atom. The average dipole moment of TIP4P-FQ bulk phases at varying temperatures is known but, as with the density, a profile of the average dipole moment is needed to characterize a multiphase environment.

### 3.5.1 Identification of Solid and Liquid Phases

The same time and length slice intervals used for the density profile were also applied to the dipole profile. Dipole moments were measured in 0.05 Å slice intervals along the length of the simulation box, and results were time averaged for 25 ps. Dividing the density of the slice through the dipole moment normalized the average dipole moment in a given slice.

The same bimodal characteristic of the prismatic layering is seen in the dipole profile (Figure 3.9). In this double molecular layer, the parallel dipole component decreases to a local minimum while the perpendicular dipole component increases to a local maximum, concurrent with the local minimum of the bimodal density peak. The deconstruction of the solid-like characteristics is more difficult to chart. The solid phase double molecular layer from 23 Å to 26 Å is marked by the absence of molecules on the left and by a sharp drop in the parallel dipole moment on the right.

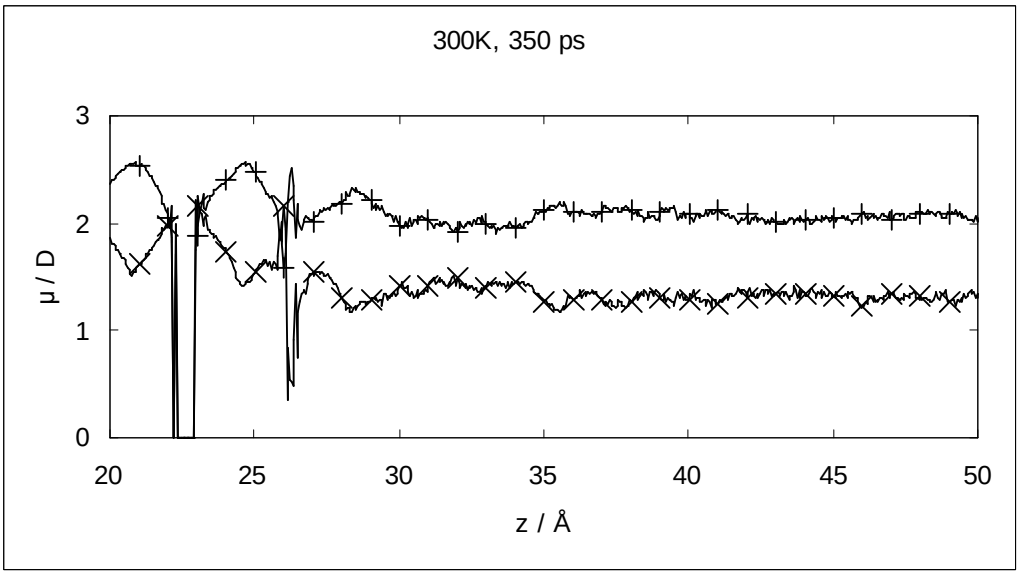


Figure 3.9. Dipole profile parallel to length of simulation (×), and perpendicular to length of simulation (+) of a stable interface along the length of the model after 350 ps of simulation at 300K, averaged over the previous 25 ps.

The interfacial area lacks any lengths absent of water molecules or precipitous changes in dipole moment when averaged over 25 ps. However, the solid-like molecular layer adjacent to the solid phase shows the same peaking and dipping behavior of the dipole moment components as the solid layer: the parallel component reaches a maximum and the perpendicular component reaches a minimum at 28 Å. The second, liquid-like layer in the interface lacks even the peaks and valleys of the solid-like layer. The sudden readjustment of dipole component values, though, suggests the termination of the interface at 34 Å. The perpendicular dipole moment is larger than the parallel dipole by about a factor of $\sqrt{2}$ in the liquid phase because the perpendicular dipole includes two perpendicular directions compared to one parallel direction.

### 3.5.2 Change in Dipole Profile with Growth

The same crystal growth at 280 K was observed at 300 ps, 400 ps, and 500 ps as used in the density analysis. (Figure 3.10) The dipole profiles support the conjecture that crystallization on the prismatic interface is a two-layer process.

Conversion of the solid-like layer in the interface, centered at section A, to the solid phase can be observed from 300 ps to 500 ps by the development of a void in the dipole moment at about 33 Å. The peaks and valleys of the dipole moment components of the liquid-like layer of section B evolve from obscurity at 300 ps to that of a solid-like interface layer by 500 ps. The molecular layer in section C seen at the 500 ps in the density profile (Figure 3.8) is difficult to distinguish from natural variations within the liquid phase. This lag in development from liquid layer to liquid-like interface layer in comparison to the equivalent density profile suggests that molecules entering the growing interface organize by translation (resulting in ordered density peaks) before they organize by rotation (resulting in ordered dipole moments).

Figure 3.10. Dipole profile parallel to length of simulation (×), and perpendicular to length of simulation (+), of a growing interface along the length of the model after 300, 400 and 500 ps of simulation at 280 K, averaged over the previous 25 ps.

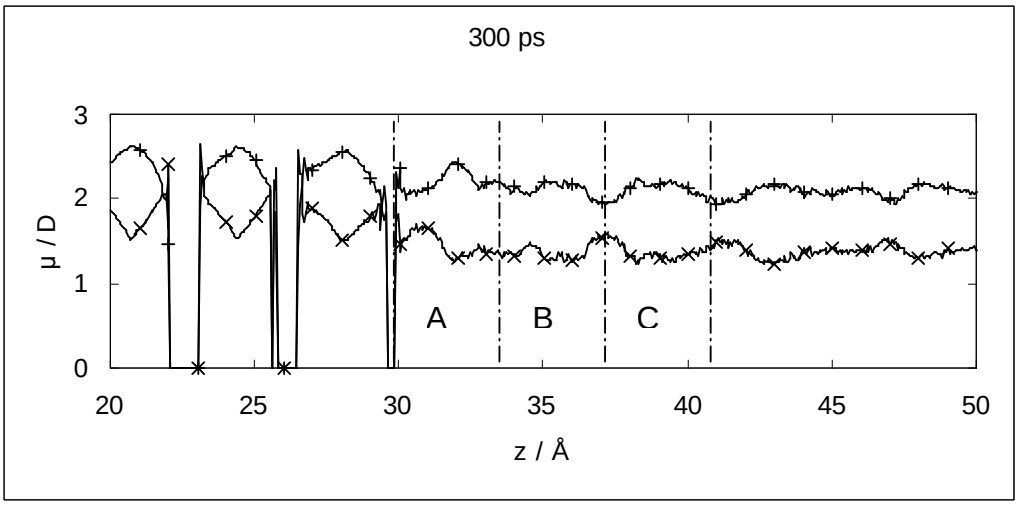
300 ps
μ / D
z / Å
A
B
C

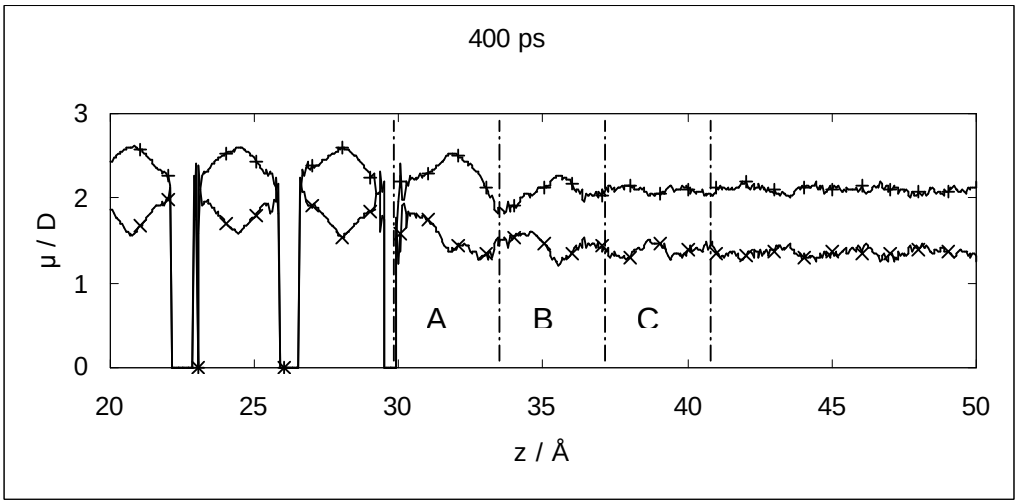
400 ps
μ / D
z / Å
A
B
C

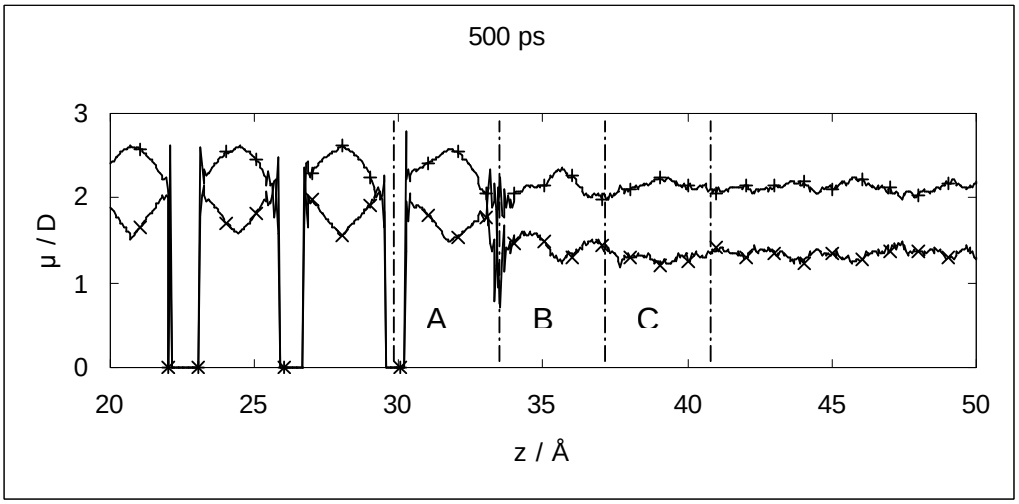
500 ps
μ / D
z / Å
A
B
C

# Chapter 4

# Conclusions

The crystallization of ice-liquid water interfaces can be investigated using the procedures and analysis presented in this thesis. Simulation of the interface response function revealed the melting temperature of the TIP4P-FQ model and the temperature of maximum velocity. The temperature of the original TIP4P-FQ model [14] is 303 ± 8 K, and its maximum interface velocity is near 1 m/s. The reparameterized TIP4P-FQ model [18] has a melting temperature of 276 K. Determination of the liquid and solid molecules allowed for characterization and location of the prismatic interface, which has a width of about 6Å. Measurement of the density and dipole profiles reveal the multi-layer mechanism of interfacial growth, and that molecule movement to the interface precedes orientation in the interface.

The interface response function for water requires long simulation times, often well beyond 500 ps as the temperature decreases, to discern net movement from natural interface fluctuation. The TIP4P-FQ model for water has been observed to exhibit a glass for several nanoseconds at 220 K [18]; this provides a lower limit for further interface response analysis. The anisotropic growth of ice suggests that the interface response function of other faces of ice will be different, and probably slower [9], than the results found here.

## 4.1 Comparison to other Models

The polarizability of the TIP4P-FQ model stabilizes the solid phase above the true melting temperature of water. Most other models predict melting temperatures below 273.15 K (Table 2.2). Comparing the properties of TIP4P-FQ discovered here to previously established properties of other models can assist in deciding which model is the appropriate choice for future simulations involving water.

### 4.1.1 Melting Temperature and Temperature of Maximum Density

The temperature of maximum density (TMD) for the original TIP4P-FQ model is 280 K [14]. While this result compares favorably with that of real water, its value relative to the model's melting temperature is inconsistent. Real water exhibits a density maximum 4 K (1.4%) above the melting temperature, an unusual phenomenon resulting from hydrogen bonding effects [61]. Unlike real water, the temperature of maximum density of TIP4P-FQ lies below the predicted melting point (-8%), similar to the results of the Broughton-Gilmer-modified SPC/E Ewald model ($T_m$= 279 ± 5 K, TMD = 260 K, -7%) [62]. A value for TMD for the reparameterized TIP4P-FQ model is around 255 K (–8%), though the density is relatively flat from 245-275 K making an accurate prediction quite difficult [63]. It is interesting that the TMD for both the TIP4P-FQ and modified TIP4P-FQ are about 20 K below their melting temperature, while the TMD for the TIP4P model, 258 K [64], is at least 20 K above the melting temperature. Most other water models predict TMD to be too high above the melting point, including SPC/E (TMD = 235 K, 4%) [65], TIP4P (TMD = 250 K, 5%) [66], and TIP5P (TMD = 277 K, 3%) [67]. Note that TIP5P was designed specifically to

produce accurate density profiles of water for large temperature and pressure ranges. The undesirable characteristic that TIP4P-FQ possesses a TMD below the melting temperature should be noted for relevant situations.

The inclusion of polarizability, at least when using fluctuating charge models, has been shown to lead to an accurate TMD [18,68]. The higher TMD for fluctuating charge models comes about because the density is much more temperature dependent and goes through the density maximum over a narrower range of temperatures. This implies that the interactions for fluctuating charge models are stronger than for the corresponding non-polarizable models. In fact, even though at 298 K the potential energy of the various models is about the same (-10 kcal/mol), the polarizable models have an increased effective interaction because a self-polarization term is added to the energy [69]. The self-polarization term is fairly large for the TIP4P-FQ model (5.7 kcal/mol) [14] making the interactions effectively much stronger. The strengths of interactions are consistent with those of liquid water, as demonstrated by the TMD. For the ice phase, the polarization energy is larger due to the larger dipole moment (see [14] and Figure 3.9), and the interactions are accordingly enhanced more for the ice phase than the liquid phase. The solid phase is stabilized more than the liquid by the addition of polarizability, enough that the melting temperature exceeds the TMD.

### 4.1.2 Temperature of Maximum Velocity

Data that provides part of the interface response function has been explored, without invoking the concept of the IRF, for one other water model: the TIP6P model. Nada and Furukawa [9] calculated the velocities of seven temperatures between 269 K and 287 K (Figure 2.6). Their linear relation fitted to the data suggests zero interface

velocity at a melting temperature of 283 K. Their fastest interfacial growth occurs at the lowest temperature simulated, 269 K.

The lack of evidence of decreasing velocity within this interval makes the fitting of the Wilson-Frenkel relation difficult. However, based on the melting temperature, the matching interval for the TIP4P-FQ IRF, from 290 K to 310 K, yields similar results (Figure 3.5). At about 15 K below the melting point, the velocity for TIP6P is about 0.5 m/s, while the velocity for TIP4P-FQ is 0.45 m/s. The Wilson-Frenkel fit for TIP4P-FQ predicts a velocity 0.54 m/s. Both interface response functions could be interpreted as linear relationships in this interval. The excellent similarity between TIP6P, a model specifically parameterized for temperatures near water's true melting point, and the polarizable TIP4P-FQ model, suggest that the IRF of water models are somewhat resistant to dramatic changes in model geometry and parameterization.

Experimental growth velocities are typically overestimated by molecular simulation, but usually remain within an order of magnitude. The velocity predicted by Hallett [42] at the lowest experiment undercooling, 20 K, is about 0.24 m/s, which is no more than a factor of four smaller than the prediction from the Wilson-Frenkel equation fitted to our simulation data. The fact that the Hallett relation is a positive polynomial function (Equation 2.20) while the Wilson-Frenkel equation is a negative exponential function (Equation 2.21) is insignificant; it can be attributed to the very small interval of supercooled temperatures available using experimental methods.

The temperature at which the maximum growth velocity occurs relative to the melting temperature, $T(v_{max})/T_m$ , is around 0.86 for the data produced here; this value corresponds well to values of around 0.82 for silicon [70], a similarly tetrahedrally coordinated open crystal structure.

### 4.1.3 Prismatic Growth Mechanism

Nada and Furukawa also investigated the growth mechanism of the prism face of ice [9]. An order parameter based on the ratio of fully coordinated liquid and solid water molecules was created, and the simulation box divided such that each slice would contain one prismatic layer if the entire system were ice. When growth occurred at the layer adjacent to bulk ice, growth was also seen to a lesser extent in the next layer as well. This concurs with the density and dipole profiles of the growing interface for TIP4P-FQ, which suggest that as the first solid-like layer is orienting into a tetrahedral coordination, the adjacent liquid-like layer is translating into place. Growth for the basal face of TIP6P ice showed no such two-layer system, but instead grew layer-by-layer [9]. Prismatic growth is faster than basal growth due to this difference in growth mechanisms.

## 4.2 Future Applications: Natural Gas Hydrates

Methane hydrates consist of a crystalline arrangement in which individual methane molecules are surrounded by water "cages." The methane is not chemically bonded with the water, but is stabilized by van der Waals forces [4]. Methane hydrates are invariably found in the pores of rock and clay under permafrost and on the ocean floor. The highest concentrations of hydrates are found near natural gas deposits and at tectonic plate boundaries. It is estimated that a 1% recovery of American hydrate deposits would double the current US natural gas supply [71]. Indeed, total world energy reserves in hydrates are thought to be double that of total conventional fossil

fuel energy reserves [72]. Conversely, hydrates can be a safety hazard by clogging wet gas transmission lines and an environmental danger caused by freely releasing methane to the atmosphere upon dissolution.

Control of this double-edged sword does not come easily. Thermodynamically, the dissociation of a methane hydrate requires only 15% of the energy recovered in methane gas [4], but current extraction methods (depressurization, thermal stimulation, and inhibition) are slow or ineffective for this low concentration resource. Injecting gas transmission lines with hydrate-inhibiting methanol is expensive, and the effect of receding permafrost on the methane hydrate underneath is not fully characterized. An increased understanding of the kinetics of hydrate formation and dissociation is necessary if these processes are to be better appreciated. While hydrate deposits exist on a geologic scale, modeling microscale characteristics and determining molecular-scale properties will provide important information to allow accurate macroscale predictions to be made [4]. Molecular scale computer simulations of hydrate formation and dissociation are much easier to define and control than experiments for which kinetic measurements are problematic [73-75]. Previous simulations of hydrate-liquid systems have included the use of hydrate seed crystal in the bulk liquid to determine critical cluster size [40].

### 4.2.1 Hydrate Structure and Occupancy

Clathrate hydrates form from water and non-stoichiometric amounts of small, non-polar molecules. Three hydrate structures are known: sI, sII, and sH. Only the first two have been observed in nature, and sI, which has ice cages small enough to stabilize methane, is by far the most common.

The sI hydrate is of the space group Pm3m. The unit cell consists of 46 water molecules and a maximum of 8 guest molecules. The water molecules are configured into 8 cages, 2 of them dodecahedrons with 12 pentagonal faces ($5^{12}$), and 6 of them tetrakaidecahedrons with 12 pentagonal faces and 2 hexagonal faces ($5^{12}6^2$) (Figure 4.1). The tetrakaidecahedrons share hexagonal faces, and their rotational symmetric axes lie in three perpendicular directions. The dodecahedrons are located in the spaces between the mesh of tetrakaidecahedrons (Figure 4.2).

The cages made by the sI structure allow guest molecules larger than 1.8 Å but smaller than 2.2 Å. These guest molecules include not only methane, but also nitrogen, oxygen, and argon. At an average 96% occupancy rate, a kilogram of sI hydrate can contain 187 liters of methane gas at atmospheric pressure.

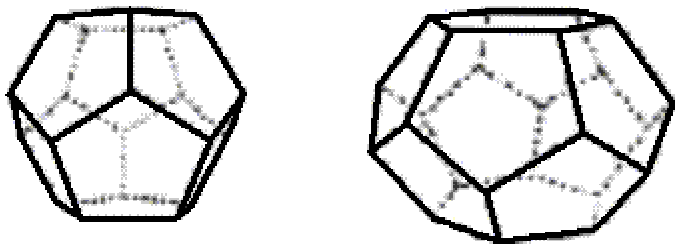

Figure 4.1. Structure of dodecahedron ($5^{12}$, left) and tetrakaidecahedrons ($5^{12}6^2$, right) hydrate cages.

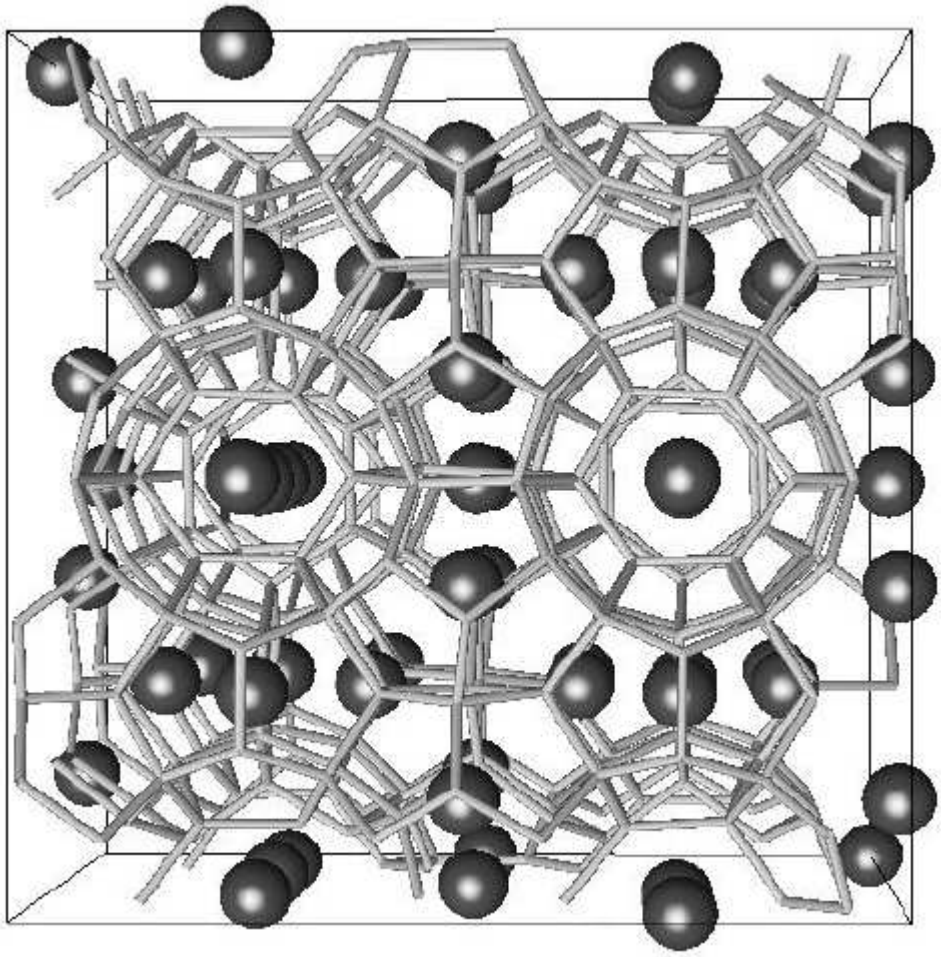

Figure 4.2. Hydrate sI structure. Note the three directions of the tetrakaidecahedrons rotational axes: horizontal along the page (2 rows, top and bottom of figure), vertical along the page (1 column, center of figure) and perpendicular to the page (2 rows, center of figure). (Source: [40])

### 4.2.2 Potential Simulation Scenarios

A simple extension of the ice-water-ice system for hydrates would involve a hydrate-water/methane-hydrate system. Methane molecules are non-polar and have no charge. They can be modeled as a single point with a Lennard-Jones interaction potential; this model potential includes the van der Waals forces that stabilize hydrates. The

dimensions of the box would be modified to accommodate hydrate structures with zero net dipole. It has been recently determined that empty hydrates breakup much faster than fully occupied hydrates, and that methane diffusion from the crystal is the rate-limiting step to hydrate breakup [76]. Consequently, the methane/water ratio in the system is equal to that of a fully occupied hydrate crystal: 8 to 46. The interface response function should not only include temperature, but also pressure as a factor in interfacial growth; hydrates typically form in nature at temperatures slightly above the melting point of water and at moderate pressures (on the order of tens of atmospheres). Formation of complete hydrate cages would verify the usefulness of the TIP4P-FQ model for hydrate simulation.

Another potential opportunity is to remove some of the periodic boundaries of the simulation box and control the box's dimensions, mimicking the actual dimension of a micropore. In small pores, the fluid-wall forces shift the thermodynamic conditions for phase transitions, encourage adsorption, and create interesting transport properties. Adsorption models specifically derived for micropores, such as the Dubinin and Radushkevich model and Sing's $\alpha_s$ method, are empirical in nature and poor for prediction [77]. Consequently, simulations using water models must currently be used on a case-by-case basis. No molecular-scale studies exist regarding the effect of pore size and surface characteristics on the kinetics of hydrate growth and dissolution.

Unique surfaces can be applied to the boundary restrictions as well. Surfaces can inhibit [74,75,78,79] or encourage hydrate growth depending on interactions of the exposed atoms and the water molecules of the hydrate. For the clay Na-montmorillonite, the methane guest can lie in a ring of oxygen atoms on the clay surface and be surrounded by an "umbrella" clathrate-like structure of water molecules

[80]. Hydrates are often found in the pore spaces of montmorillonites and other silicates. Kinetic inhibitors, which are often discovered by chance in the laboratory, can also be investigated by simulation and the method of halting the growth mechanism can be determined.

The numerous ice forms and the interactions that water has with nearly every aspect of this planet make countless opportunities available for simulation. Awareness of the limitations and disparaging properties of the many water models is key in choosing which models to use for a given simulation environment.

# References


[1] J. Hallet and G. Isaac, "Aircraft Icing in Glaciated and Mixed Phase Clouds", American Institute of Aeronautics and Astronautics 40th Aerospace Sciences Meeting and Exhibit, 2002-0677 (2002).

[2] S. Sigurgisladottir, H. Ingvarsdottir, O. J. Torrissen, M. Cardinal, and H. Hafsteinsson, "Effects of freezing/thawing on the microstructure and texture of smoked Atlantic salmon (*Salmo salar*)", Food Research International **33**, 857 (2000)

[3] A. A. Antson, D. J. Smith, D. I. Roper, S. Lewis, L. S. Caves, C. S. Verma, S. L. Buckley, P. J. Lillford, and R. E. Hubbard, "Understanding the mechanism of ice binding by type III antifreeze proteins", Journal of Molecular Biology **305**, 875 (2001).

[4] E. D. Sloan, *Clathrate Hydrates of Natural Gases*, (Marcel Dekker, Inc., New York, 1998).

[5] Ph. Wernet, et al., "The Structure of the First Coordination Shell in Liquid Water," Science **304**, 995 (2004).

[6] J. D. Smith, C. D. Cappa, K. R. Wilson, B. M. Messer, R. C. Cohen, R. J. Saykally, "Energetics of Hydrogen Bond Network Rearrangements in Liquid Water", Science **306**, 851 (2004).

[7] A. Nilsson, et al., "Comment on 'Energetics of Hydrogen Bond Network Rearrangements in Liquid Water'", Science **308**, 793a (2005).

[8] J D. Smith, C. D. Cappa, B. M. Messer, R. C. Cohen, R. J. Saykally, "Response to Comment on 'Energetics of Hydrogen Bond Network Rearrangements in Liquid Water'", Science **308**, 793b (2005).

[9] H. Nada and Y. Furukawa, "Anisotropy in growth kinetics at interfaces between proton-disordered hexagonal ice and water: A molecular dynamics study using the six-site model of $H_2O$", Journal of Crystal Growth **283**, 242 (2005).

[10] B. Guillot, "A reappraisal of what we have learnt during three decades of computer simulations on water", Journal of Molecular Liquids **101**, 219 (2002).

[11] T. Werder, J. H. Walther, R. L. Jaffe, T. Halicioglu, F. Noca, and P. Koumoutsakos, "Molecular dynamics simulations of contact angles of water droplets in carbon nanotubes", Nano Letters **1**, 697 (2001).

[12] F. Allen, et. al. "Blue Gene: A vision for protein science using a petaflop supercomputer", IBM Systems Journal **40**, 310 (2001).

[13] A. P. Heiner, A. P., L. Kuutti, and O. Teleman, "Comparison of the interface between water and four surfaces of native crystalline cellulose by molecular dynamics simulations", Carbohydrate Research **306**, 205 (1998).

[14] S. W. Rick, S. J. Stuart, B. J. Berne, "Dynamical fluctuating charge force fields: Application to liquid water", Journal of Chemical Physics **101**, 6141 (1994).

[15] A. V. Gubskaya and P. G. Kusalik, "The total molecular dipole moment for liquid water", Journal of Chemical Physics **117**, 5290 (2002).

[16] S. J. Suresh and V. M. Naik, "Hydrogen bond thermodynamic properties of water from dielectric constant data", Journal of Chemical Physics **113**, 9727 (2000).

[17] E. R. Batista, S. S. Xantheas and H. Jonsson, "Molecular multipole moments of water molecules in ice Ih", Journal of Chemical Physics **109**, 4546 (1998).

[18] S. W. Rick, "Simulations of ice and liquid water over a range of temperatures using the fluctuating charge model", Journal of Chemical Physics **114**, 2276 (2001).

[19] C. J. Tymczak and John R. Ray, "Interface response function for a model of sodium: A molecular dynamics study", Journal of Chemical Physics **92**, 7520 (1990).

[20] O. A. Karim and A. D. J. Haymet, "The ice/water interface", Chemical Review Letters **138**, 531 (1987).

[21] H. Nada and Y. Furukawa, "Anisotropic Properties of Ice/Water Interface: A Molecular Dynamics Study", Japanese Journal of Applied Physics **34**, 583 (1995).

[22] J. A. Hayward and A. D. J. Haymet, "The ice/water interface: Molecular dynamics simulations of the basal prism, $\{2\bar{1}10\}$, and $\{20\bar{2}1\}$ interfaces of ice Ih", Journal of Chemical Physics **114**, 3713 (2001).

[23] T. Byrk and A. D. J. Haymet, "The Ice 1h/water interface of the SPC/E model: Molecular dynamics simulations of the equilibrium basal and prism interfaces", Journal of Chemical Physics **117**, 10258 (2002).

[24] M. P. Allen and D. J. Tildesley, *Computer Simulation of Liquids*, (Clarendon Press, Oxford, 1990).

[25] L. Verlet, "Computer "Experiments" on Classical Fluids. I. Thermodynamical Properties of Lennard-Jones Molecules", Physics Review **159**, 98 (1967).

[26] S. Nosé, "A molecular dynamics method for simulations in the canonical ensemble", Molecular Physics **52**, 255 (1984).

[27] H. C. Andersen, “Molecular dynamics simulations at constant pressure and/or temperature”, Journal of Chemical Physics **72**, 2384 (1980).

[28] H. J. C. Berendsen, J. P. M. Postma, W. F. van Gunsteren, A. DiNola, and J. R. Haak, “Molecular dynamics with coupling to an external bath”, Journal of Chemical Physics **81**, 3684 (1984).

[29] H. Nada, J. P. J. M. van der Eerden, “An intermolecular potential model for the simulation of ice and water near the melting point: A six-site model of $H_2O$”, Journal of Chemical Physics **118**, 7401 (2003).

[30] J. L. F. Abascal and C. Vega, “A general purpose model for the condensed phases of water: TIP4P/2005”, Journal of Chemical Physics **123**, 234505 (2005).

[31] J. D. Bernal and R. H. Fowler, “A Theory of Water and Ionic Solution, with Particular Reference to Hydrogen and Hydroxyl Ions”, Journal of Chemical Physics **1**, 515 (1933).

[32] N. Metropolis, A. W. Rosenbluth, M. N. Rosenbluth, A. H. Teller and E. Teller, “Equation of State Calculations by Fast Computing Machines”, Journal of Chemical Physics **21**, 1087 (1953).

[33] C. Vega, E. Sanz, and J. L. F. Abascal, “The melting temperature of the most common models of water”, Journal of Chemical Physics **122**, 114507 (2005).

[34] B. W. Arbuckle and P. Clancy, “Effect of the Ewald sum on the free energy of the extended simple point charge model for water”, Journal of Chemical Physics **116**, 5090 (2002).

[35] E. Sanz, C. Vega, J. L. F. Abascal, and L. G. MacDowell, “Phase Diagram of Water from Computer Simulation”, Physical Review Letters **92**, 255701 (2004).

[36] F. H. Stillinger and A. Rahman, “Molecular Dynamics Study of Temperature Effects on Water Structure and Kinetics”, Journal of Chemical Physics **57**, 1281 (1972).

[37] J. A. Hayward and J. R. Reimers, “Unit cells for the simulation of hexagonal ice”, Journal of Chemical Physics **106**, 1518 (1997).

[38] P. V. Hobbs, *Ice Physics*, (Clarendon Press, Oxford, 1974).

[39] M. J. Uttormark, “Melting Kinetics of Small Crystalline Clusters in the Liquid by Molecular dynamics”, Ph.D. Dissertation, Cornell University, (1992).

[40] L. A. Báez, “Computer Simulation of Early-Stage Crystal Growth and Dissolution”, Ph.D. Dissertation, Cornell University, (1996).

[41] A. K. Soper and M. G. Phillips, “A new determination of the structure of water at 25°C” Chemical Physics **107**, 47 (1986).

[42] J. Hallet, “Experimental Studies of the Crystallization of Supercooled Water”, J. Atmospheric Sciences **21**, 671 (1964).

[43] D. Frenkel and B. Smit, *Understanding molecular simulation: from algorithms to applications*, (Academic Press Inc., San Diego, 1996).

[44] D. Frenkel and A. J. C. Ladd, “New Monte Carlo method to compute the free energy of arbitrary solids. Application to the fcc and hcp phases of hard spheres”, Journal of Chemical Physics **81**, 3188 (1984).

[45] G. T. Gao and X. C. Zeng, “The melting temperature of proton-disordered hexagonal ice: A computer simulation of 4-site transferable intermolecular potential model of water”, Journal of Chemical Physics **112**, 8534 (2000).

[46] J. Wang, S. Yoo, and J. Bai, “Melting temperature of ice $I_h$ calculated from coexisting solid-liquid phases”, Journal of Chemical Physics **123**, 036101 (2005).

[47] Y. Koyama, H. Tanaka, G. Gao and X. C. Zeng, “Melting points and thermal expansivities of proton-disordered hexagonal ice with several model potentials”, Journal of Chemical Physics **121**, 7926 (2004).

[48] S. Yoo and X. C. Zeng, “The melting lines of model silicon calculated from coexisting solid-liquid phases”, Journal of Chemical Physics **120**, 1654 (2004).

[49] M.O. Thompson, G. J. Galvin, J. W. Mayer, P. S. Peercy, J. M. Poate, D. C. Jacobson, A. G. Cullis and N. G. Chew, “Melting Temperature and Explosive Crystallization of Amorphous Silicon during Pulsed Laser Irradiation”, Physical Review Letters **52,** 2360 (1984).

[50] A. Chojnacka and M. O. Thompson, in *Growth, Evolution and Properties of Surfaces, Thin Films and Self-Organized Structures*, edited by S. C. Moss, D. B. Pokers, and D. Ila, MRS Symposia Proceedings No. 648 (Materials Research Society, Pittsburgh, 2001), p. P11.12.1-8.

[51] H. Nada and Y. Furukawa, “Anisotropy in structural transitions between basal and prismatic faces of ice studied by molecular dynamic simulation”, Surface Science **446**, 1 (2000).

[52] T. Ikeda-Fukazawa, K. Kawamura, “Molecular-dynamics studies of surface of ice Ih”, Journal of Chemical Physics **120**, 1395 (2004).

[53] H. Nada and Y. Furukawa, “Anisotropic growth kinetics of ice crystals from water studied by molecular dynamics simulation”, Journal of Crystal Growth **169**, 587, (1996).

[54] H. Nada and Y. Furukawa, “Anisotropy in Molecular-Scaled Growth Kinetics at Ice-Water Interfaces”, Journal of Physical Chemistry B **101**, 6163 (1997).

[55] H. R. Pruppacher, “Self-Diffusion Coefficient of Supercooled Water”, Journal of Chemical Physics **56**, 101 (1972).

[56] F. X. Prielmeier, E. W. Lang, R. J. Speedy, and H.-D. Lüdemann, “Diffusion in supercooled water to 300 MPa”, Physical Review Letters **59**, 1128 (1987).

[57] D. Eisenberg and W. Kauzmann, *Structure and Properties of Water*, (Oxford University Press, New York and Oxford, 1969).

[58] D. A. Kofke, “Gibbs-Duhem Integration: A New Method for Direct Evaluation of Phase Coexistence by Molecular Simulation”, Molecular Physics **78**, 1331 (1993).

[59] J. B. Sturgeon and B. B. Laird, “Adjusting the melting point of a model system via Gibbs-Duhem integration: Application to a model of aluminum”, Physical Review B **62**, 14720 (2000).

[60] B. F. Nicholson, P. Clancy, and S. W. Rick, “The interface response function and melting point of the prism interface of ice $I_h$ using a fluctuating charge model (TIP4P-FQ)”, J. Crystal Growth (accepted).

[61] H. Tanaka, “Simple Physical Explanation of the Unusual Thermodynamic Behavior of Liquid Water”, Physical Review Letters **80**, 5750 (1998).

[62] L. A. Báez and P. Clancy, “Phase Equilibria in Extended point Charge Ice-Water Systems”, Journal of Chemical Physics **103**, 9744 (1995).

[63] S. W. Rick, unpublished results (2005).

[64] W. L. Jorgensen and C. Jensen, “Temperature dependence of TIP3P, SPC, and TIP4P water from NPT Monte Carlo simulations: Seeking temperatures of maximum density”, Journal of Computational Chemistry **19**, 1179 (1998).

[65] L. A. Báez and P. Clancy, “Existence of a Density Maximum in SPC/E-modeled Water”, Journal of Chemical Physics **101**, 9837 (1994).

[66] F. Sciortino, and S. Sastry, “Sound propagation in liquid water: The puzzle continues”, Journal of Chemical Physics **100**, 3881 (1994).

[67] M. W. Mahoney and W. L. Jorgensen, "A five-site model for liquid water and the reproduction of the density anomoly by rigid, nonpolarizable potential functions", Journal of Chemical Physics **112**, 8910 (2000).

[68] B. Chen, J. Xing, and J. I. Siepmann, “Development of Polarizable Water Force Fields for Phase Equilibrium Calculations”, Journal of Physical Chemistry B **104**, 2391 (2000).

[69] H.J.C. Berendsen, J.R. Grigera, and T.P. Straatsma, “The missing term in effective pair potentials”, Journal of Physical Chemistry **91**, 6269 (1987).

[70] E. J. Albenze, M. O. Thompson, and P. Clancy, “Atomistic computer simulation of explosive crystallization in pure silicon and germanium”, Physical Review B **70**, 094110 (2004).

[71] DOE Website, “Methane Hydrates – The Gas Resource of the Future” http://www.fossil.energy.gov/programs/oilgas/hydrates/ Accessed March 4, 2004.

[72] K. Kvenvolden, “Methane hydrate – A major reservoir of carbon in the shallow Geosphere?”, Chemical Geology **71**, 41 (1988).

[73] R. Inoue, H. Tanaka, and K. Nakanishi, “Molecular dynamics simulation study of the anomalous thermal conductivity of clathrate hydrates”, Journal of Chemical Physics **104**, 9569 (1996).

[74] E. Freer and E. Sloan, “An Engineering Approach to Kinetic Inhibitor Design Using Molecular Dynamics Simulations”, Annals of the New York Academy of Sciences **715**, 651 (1994).

[75] K. Yasuoka and S. Murakoshi, “Molecular Dynamics Simulation of Dissociation Process for Methane Hydrate”, Annals of the New York Academy of Sciences **715**, 678 (1994).

[76] N. J. English, J. K. Johnson, and C. E. Taylor, “Molecular-dynamics simulations of methane hydrate dissociation”, Journal of Chemical Physics **123**, 244503 (2005).

[77] R. Cracknell, K. E. Gubbins, M. Maddox, and D. Nicholson, “Modeling Fluid Behavior in Well Characterized Porous Materials”, Accounts of Chemical Research **28**, 281 (1995).

[78] T. Carver, M. Drew, and P. M. Rodger, “Configuration-Biased Monte Carlo Simulations of poly(vinylpyrrolidone) at a Gas Hydrate Crystal Surface”, Annals of the New York Academy of Sciences **715**, 658 (1994).

[79] M. Storr and P. Rodger, “A Molecular Dynamics Study of the Mechanism of Kinetic Inhibition”, Annals of the New York Academy of Sciences **715**, 669 (1994).

[80] S. Park, and G. Sposito, “Do Montmorillonite Surfaces Promote Methane Hydrate Formation? Monte Carlo and Molecular Dynamics Simulations,” Journal of Physical Chemistry B **2003**, 2281 (2003).